PREACTIVATED THIOMER MUCOADHESIVE MICELLES FOR ANTERIOR OPHTHALMIC DRUG DELIVERY

PREACTIVATED THIOMER MUCOADHESIVE MICELLES FOR ANTERIOR OPHTHALMIC DRUG DELIVERY

By

TAYLOR GOOTREY, B.ENG.BIOSCIENCES.

A Thesis

Submitted to the School of Graduate Studies

In the Partial Fulfillment of the Requirements

For the Degree

Master of Applied Science

McMaster University

MASTER OF APPLIED SCIENCE (2021) McMaster University

(Chemical Engineering) Hamilton, Ontario

TITLE: Preactivated Thiomer Mucoadhesive Micelles for Anterior Ophthalmic Drug Delivery

AUTHOR: Taylor Goostrey, B.Eng. & Biosci. (McMaster University)

SUPERVISOR: Professor Heather Sheardown

NUMBER OF PAGES: xvii, 90

ABSTRACT

Effective delivery of drugs to the anterior segment of the eye is notoriously inefficient due to the anatomical barriers in place. Topical administration is the most common method of drug delivery to the anterior segment. When applied to the ocular surface, topical solutions encounter barriers such as lacrimal drainage, rapid tear turnover, and reflex blinking which result in < 5% of instilled therapeutic reaching the intended tissue. One potential method to evade some of these anatomical barriers and improve the delivery of therapeutics is the use of mucoadhesive nanoparticles. These materials are designed to encapsulate a relevant ocular therapeutic and provide a means of maintaining the vehicle on the ocular surface by adhering to the mucin layer of the tear film.

To this end, the work presented herein describes the design, characterization, and testing of a novel mucoadhesive polymeric nano-micelle ocular drug delivery system. The base polymer used was selected from a system that has been previously used in the Sheardown Lab. It was composed of poly(D,L-lactide)-*block*-poly(methacrylic acid-*co*-3-(acrylamido)phenylboronic acid) (PLA-*b*-P(MAA-*co*-3-AAPBA); LMP-20). The formulation was modified to replace the 3-AAPBA monomer, which contains phenyl boronic acid as the mucoadhesive component, with a preactivated thiol monomer (pyridyl disulfide ethyl methacrylate; PDSMA) to generate a novel polymer (LMS-20) to investigate the potential for drug incorporation and mucoadhesion. Modifications of the polymer were made with

small thiol molecules cysteamine (Cys; LMC-20), glutathione (GSH; LMG-20), and N-acetyl cysteine (NAC; LMA-20) with a goal of reducing cytotoxicity associated with the 2-pyridinethione leaving group.

Synthesis of the PDSMA monomer, LMS-20 and LMP-20 polymers, and modified polymers LMC-20, LMG-20, and LMA-20 were confirmed by ^{1}H NMR. LMA-20 was chosen for further examination as it contained the most relevant thiol modification for ocular applications and was capable of nanoprecipitation to form aqueous micelles with previously developed methods. Micelles were formed from LMA-20 and LMP-20, with spherical morphology as confirmed by TEM. Effective diameters of 64 ± 5 nm and 72 ± 3 nm are reported for LMA-20 and LMP-20, respectively, as confirmed by DLS. Critical micelle concentration for LMA-20 of 217 mg/L was found via a pyrene fluorescence study, significantly lower than the concentration of intended application. LMA-20 and LMP-20 are predicted to be mucoadhesive based on results of zeta-potential studies. However, oscillatory rheology studies were inconclusive based on a negative rheological synergism. LMA-20 micelles loaded with 0.16% (w/w) Cyclosporine-A were able to provide sustained release of drug up to 3 days *in vitro*. These results suggest the possible future use of these preactivated thiomer-based materials for the delivery of therapeutics to the anterior segment.

ACKNOWLEDGEMENTS

There are so many people I would like to thank who have provided me with the support and encouragement to complete this body of work. First, to my supervisor Dr. Heather Sheardown, for giving me this exceptional experience. From the first time I met you I knew you were going to be a superb mentor. Thank you for the countless opportunities, not only giving me the freedom to perform the research presented herein, but for the ARVO and WBC conferences, Lab2Market program, and all the lab group outings, it has been a truly unforgettable few years.

I would like to thank many members of the Sheardown Lab throughout my time who have provided both the wonderfully collaborative work environment we all share, as well as their friendship. To Mitch, who's been like a brother to me these past 2 years, thanks for teaching me how to brew and getting me hooked on fantasy football. To Nicole, who kept my adventurous spirit alive whether through trips to Fairweather or Killarney, thanks for being a true friend. To Jenn, Emily-Anne, Ridhdhi, and Ben thanks for all the good times and everything you've taught me along the way. To Fran, thank you for pushing me to pursue the Lab2Market program, it ended up being a highly beneficial experience and was great to work alongside you. To Lina, thank you for continuously teaching me new ways to troubleshoot a problem and for all the support with drug release studies and running TEM. To Karim, thank you for all the support with drug release studies and running HPLC. To Talena, thank you for teaching me everything I know about

organic chemistry and laboratory techniques, I would have never been able to complete this project without your expertise.

Finally, a huge thank you to my family and to Dom who have put up with me being in school for so long and continue to support me.

TABLE OF CONTENTS

LIST OF FIGURES

LIST OF TABLES

LIST OF ABBREVIATIONS

2-Mercaptonicotinic acid	2-MNA
3-(Acrylamido)phenylboronic acid	3-AAPBA
Acetonitrile	ACN
Analysis of Variance	ANOVA
Azobis(isobutyronitrile)	AIBN
Chitosan	CS
Critical Micelle Concentration	CMC
Curcumin	CUR
Cyclosporine-A	Cyc-A
Cysteamine	Cys
Cysteine	cys
Deuterated Chloroform	$CDCl_3$
Deuterated Water	D_2O
Dextran	Dex
Dichloromethane	DCM
Dimethyl Sulfoxide	DMSO
Discovery Hybrid Rheometer	DHR
Drug Loading	DL
Dry Eye Disease	DED
Dynamic Light Scattering	DLS
Entrapment Efficiency	EE
Ethyl Acetate	EtOAc
Gel Permeation Chromatography	GPC
Glutathione Disulfide Ethyl Methacrylamide	GDSMA
High Pressure Liquid Chromatography	HPLC
Hyaluronic Acid	HA
L-Glutathione	GSH
Methacrylic Acid	MAA
Methanol	MeOH
Molecular Weight	MW
Molecular Weight Cut Off	MWCO
Monomer from Scratch	MFS
N-(Methacryloyloxy)succinimide	NMAS
N,N-Diisopropylethylamine	DIPEA
N-Acetyl Cysteine	NAC
Nanoparticle	NP
Nanostructured Lipid Carrier	NLC
N-Methacryloyl Cystamine	MAC
Nuclear Magnetic Resonance	NMR
Phenylboronic Acid	PBA

Phosphate Buffered Saline	PBS
PLA-*b*-P(MAA-*co*-3-AAPBA)	LMP
PLA-*b*-P(MAA-*co*-PDSMA)	LMS
Poly(Acrylic Acid)	PAA
Poly(Ethylene Glycol)	PEG
Poly(D,L-Lactide)	PLA
Poly(Vinyl Pyrrolidone)	PVP
Polydispersity Index	PDI
Porcine Stomach Mucin	PSM
Post-Polymerization Modification	PPM
Pyridyl Disulfide	PDS
Pyridyl Disulfide Alcohol	PDSOH
Pyridyl Disulfide Ethyl Methacrylate	PDSMA
Reversible Addition-Fragmentation Chain-Transfer	RAFT
Sodium Alginate	SA
Standard Deviation	SD
Tetrahydrofuran	THF
Thin Layer Chromatography	TLC
Transmission Electron Microscopy	TEM
Tripolyphosphate	TPP

1. INTRODUCTION

1.1. Nanocarrier Mucoadhesion as an Ocular Drug Delivery Mechanism

Drug delivery to the anterior segment of the eye is notoriously difficult due to the normal anatomical and physiological barriers. Pre-corneal mechanisms such as reflex blinking, tear turnover, and nasolacrimal drainage [1], the mechanical barrier of the cornea [2], and the tight junctions, lymphatics, and vasculature of the conjunctiva [3], all present barriers to overcome in the development of ocular drug delivery systems.

The treatment of ocular conditions of the anterior segment can be achieved using a host of techniques: intracameral or sub-conjunctival injections, systemic circulation, or topical administration [4]. While intracameral and sub-conjunctival injections can overcome certain anatomical barriers to drug delivery providing enhanced bioavailability, the requirement for a health care professional to apply the treatment, the risk of complications, and low patient compliance present drawbacks [5]. Systemic administration is avoided due to the blood-aqueous barrier which limits drugs from being absorbed from the blood into the ocular environment, resulting in low levels of delivery to the eye and large doses of drug reaching other organs in the body, inducing possible toxic effects [4]. Topical administration remains the most common method of drug delivery to the anterior segment due to its higher patient compliance and ease of application, however it often results in a low bioavailability of < 5% due to the ocular barriers [6].

Commercial formulations of topical ocular therapeutics are typically aqueous solutions, suspensions, or emulsions of drug [7]. When applied topically, these formulations quickly mix with the ocular tear fluid and are cleared via reflex blinking, tear turnover, and nasolacrimal drainage [7]. Therefore, formulations which can overcome some of these barriers through enhanced ocular retention while maintaining the ability to be applied topically are of increasing interest in the field.

Improved bioavailability of ocular therapeutics can be obtained through innovations such as *in situ* gels, drug-laden contact lenses, and nanoparticles (NPs). *In situ* gels are typically polymer formulations which exist as a liquid until topical administration, which results in a transformation to a solid hydrogel based on for example pH, electrolyte composition, or temperature difference (or a combination thereof) between that of the solution and that of the tear film [8]. This allows for the entrapment of drug and sustained release over time, however patient compliance is often lower than that of eye drops due to lower comfort and convenience [8]. Contact lenses laden with drug can be applied directly to the ocular surface allowing for improved residence time and the added benefit of decades of patient compliance. The drawback is that modifications to traditional contact lenses present issues with not only current manufacturing methods, but also with optimization of modified lenses to maintain optical and mechanical properties, hydration, and oxygen transmissibility, among others [9]. In addition, this technique cannot be used for all patients as non-lens wearing patients may

not be willing to adapt. NPs, on the other hand, provide an alternative that enables the maintenance of the existing properties of eye drops, while taking advantage of tear properties such as the mucin-layer of the tear film for mucoadhesion [10]. By designing NPs with mucoadhesive properties, researchers have proposed formulations that bind intimately to the ocular mucin through covalent and non-covalent interactions to improve the residence time and bioavailability of instilled therapeutics on the ocular surface [10].

1.2. Overall Objectives

The overall research objectives of this thesis center around the design, synthesis, and testing of novel mucoadhesive polymeric nano-micelles. The fundamental objective is such that the incorporation of a novel mucoadhesive moiety has the potential to improve mucoadhesive properties while allowing for the incorporation of a broad range of drugs. The polymer chosen for the synthesis of the nano-micelle should be compatible with the ocular environment. The nano-micelle should provide improvement in the bioavailability of drug on the ocular surface over existing topical formulations. It must have the capability to encapsulate and release relevant ocular therapeutics with appropriate kinetics. In order to improve the residence time on the eye, the nano-micelle should incorporate mucoadhesive component(s) to provide enhanced targeted delivery to intended tissues.

1.3. Thesis Outline

The research presented herein has been assembled into five distinct chapters. In Chapter 1, the thesis and its objectives are introduced, along with the outline provided here. Chapter 2 provides an overview of the pertinent literature focusing specifically on anterior segment drug delivery systems, their advantages and drawbacks, and the use of nanocarriers, particularly ones containing mucoadhesive components. The materials and methods used are discussed in Chapter 3. The results of the research, including the monomer and polymer synthesis, along with composition, size, morphology, charge, mucoadhesive properties, and drug release kinetics of the polymeric nano-micelles are presented and discussed in Chapter 4. Finally, a summary with concluding remarks and recommendations for future work can be found in the Chapter 5.

1.4. Contributions to Articles

The following explains my contributions to the work presented in Chapter 2, Section 2. The work presented in Sections 2.1, 2.2, 2.3, 2.4, as well as Figures 1 and 2, comes directly from the review article co-authored by me and Ridhdhi Dave, and submitted *January 14th, 2021* to the *Journal of Controlled Release*:

T. Goostrey, R. Dave, M. Ziolkowska, S. Czerny-Holownia, T. R. Hoare, and H. Sheardown, “Ocular Drug Delivery to the Anterior Segment Using Nanocarriers: A Mucoadhesive/Mucopenetrative Perspective,” *Journal of Controlled Release*.

Written permission was obtained in writing from the *Journal of Controlled Release* prior to incorporation into this academic thesis.

2. LITERATURE REVIEW

2.1. Anatomy of the Anterior Segment

The anterior segment of the eye comprises the cornea, conjunctiva, sclera, the aqueous chamber, the iris, and ciliary bodies as well as the lens and the associated structures including the tear film [11]. The human tear film is a dynamic fluid layer that coats the ocular surface (Figure 1). Many models have been proposed to describe the composition of the tear film, with the most widely accepted being the three-layer model [12, 13]. This model describes a tear film composed of a surface lipid layer, a middle aqueous layer, and a bottom mucin-gel layer. The lipid layer consists of hydrophobic lipids produced by the Meibomian glands of the eyelid; these lipids prevent evaporation of the tear film. The aqueous layer contains a mixture of water, electrolytes, antimicrobial compounds, soluble mucins, and vitamins among other substances and is produced by the lacrimal glands. The aqueous gel layer provides a means of nourishment of the avascular cornea and helps with the removal of toxins and debris. The mucin-gel layer is composed of mostly water (>95%) but contains a vast mucin-gel structure produced by the goblet cells of the conjunctiva [14]. Mucin is a glycoprotein consisting of a peptide backbone from which long glycan chains extend, with the presence of sialic acid and sulfated residues on the glycan chains resulting in a net negative charge [14, 15]. Mucins vary in size from 0.1-40 MDa and can interact with one another through a combination of intermolecular disulfide bonds, electrostatic forces, and physical entanglement [14, 16], resulting in a characteristic gel-like structure. The mucin

layer plays a critical role in trapping large macromolecules, bacteria, and other pathogens, thereby preventing their penetration through to the ocular surface epithelium, as well as acting as a lubricant to protect the ocular epithelium from damage due to the action of blinking [17, 18].

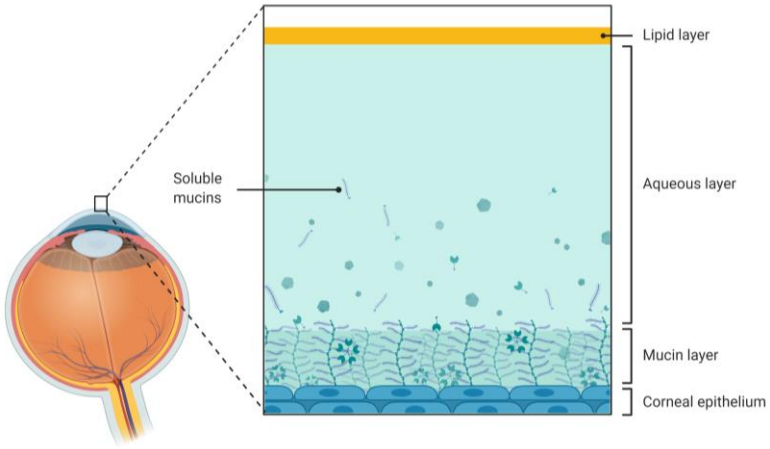

Figure 1. Structure of the tear film and its constituent layers.

The tear film sits atop the ocular surface in contact with the corneal and conjunctival epithelia. The cornea is an avascular tissue consisting of the corneal epithelium, Bowman's layer, corneal stroma, Descemet's membrane, and corneal endothelium [11, 12]. The corneal epithelium is lipophilic, consisting of 5-6 layers of epithelial cells containing tight junctions in the 2-3 layers at the apical surface [11]. The apical cell layer of the epithelium contains membrane-bound mucins with ectodomains extending nearly 500 nm into the tear film [16]. The conjunctiva coats the inner eyelid and the ocular surface over top the sclera, joining the cornea at the limbus. It is a vascular membrane composed of an epithelium, substantia

propria, and submucosa [11]. The apical cell layer of the epithelium is composed of tight junctions between cells and contains interspersed goblet cells which secrete the gel-forming mucins responsible for forming the mucin-gel layer of the tear film, while the epithelial cells contain membrane-bound mucins with ectodomains similar to the cornea [3].

2.2. Challenges in Topical Ocular Drug Delivery for Anterior Segment Diseases

Drug delivery to the anterior segment of the eye in the form of topical administration is impeded by a variety of anatomical factors, including precorneal, corneal, and conjunctival barriers as well as conjunctival blood flow and lymphatics.

Precorneal clearance mechanisms such as tear turnover or nasolacrimal drainage following topical ocular delivery contribute to the majority of the drug loss [1]. The tear film provides the first barrier to topical administration due to its high turnover rate. In a healthy eye, the tear volume ranges from 7–9 µL with a turnover rate of 0.5–2.2 µL/min [4]. An increase in volume following topical administration of ocular therapeutics in the cul-de-sac leads to reflex blinking and increased tear secretion [19], resulting in rapid drug loss from the precorneal area into the nasal cavity and ultimately the systemic circulation [20]; the latter is further enhanced by the highly vascularized walls of the nasolacrimal duct [21].

For the fraction of drug retained following tear turnover, the tight junctions in the anterior segment epithelium act to prevent the paracellular permeation of

hydrophilic drugs [3]. The small percentage of drug that permeates the conjunctival epithelium ultimately reaches the stroma where conjunctival blood capillaries and lymphatics absorb a further significant portion of drug [3]. Similar barriers exist in the cornea [2]. The superficial cells of the corneal epithelium are joined by intercellular tight junctions which limit the paracellular permeation of drug molecules [22]. The cornea also poses specific permeation barriers to multiple types of drugs. The hydrophobic nature of the corneal epithelium limits the permeation of hydrophilic drugs; conversely, the corneal stroma consisting of collagen fibers with aqueous pores allows hydrophilic drugs to pass through easily but acts as a barrier for lipophilic drugs. Consequently, drugs of all polarities have limited permeation through the cornea [23]. The sclera, which is continuous with the cornea, consists mainly of collagen with embedded proteoglycans and thus offers a similar barrier to lipophilic drugs as the corneal stroma layer [24]. However, due to the significant surface area of the sclera and its relative permeability to hydrophilic drugs, it can act as one route for hydrophilic drug delivery provided that the drug can permeate through the conjunctiva; this is the key reason subconjunctival injections are often proposed in ophthalmic drug delivery despite the patient compliance and injection risk issues involved.

As a result of these barriers and drainage mechanisms, frequent administration of eye drops is necessary to maintain a therapeutically relevant drug concentration in the tear film or at the desired site of action. However, the frequent use of highly concentrated drop solutions, in addition to being inconvenient for the patient

leading to compliance issues, may induce toxic side effects and cellular damage at the ocular surface [4]. As such, delivery systems that can enhance the residence time of a delivered drug dose in the tear film offer potential to use overall reduced drug doses while still delivering sufficient drug to the target tissues.

2.3. Mechanisms of Mucoadhesion

Several theories have been used to describe mucoadhesion of NPs with ocular surface mucins, the three most prevalent of which are (1) *adsorption*, (2) *diffusion*, and (3) *electronic* [25-30], as illustrated schematically in Figure 2. While a mucoadhesive NP is likely to exploit more than one primary mechanism to promote mucoadhesion, one is typically dominant for a particular NP type.

(1) The *adsorption theory* states that hydrogen bonding and van der Waals forces are the driving forces for mucin-particle interactions, enabling further interaction through chemisorption of mucoadhesive delivery vehicles via the formation of covalent interactions between functional groups on the vehicles and mucin. For example, NPs with surface chemistries based on poly(vinyl alcohol), hydroxyethyl methacrylate, and poly(methacrylic acid) can strongly hydrogen bond with mucin to drive mucin-NP interactions [6].

(2) The *diffusion theory* proposes that the interdiffusion of polymer chains into the mucous membrane is responsible for mucoadhesion. In this context, the shape and architecture of the polymers at the NP surface are important for establishing adhesion. The penetration rate is dependent on the diffusion

coefficient, mobility, contact time, flexibility, and nature of the polymer chains. Polymers featuring long, linear, and flexible polymeric chains (e.g. poly(ethylene glycol)) have been previously shown to facilitate improved interpenetration with mucins and thus mucoadhesion [25]. The ideal polymer molecular weight to enable adhesion depends on the type of polymer; as one example, the bioadhesive forces of poly(ethylene glycol) (PEG) increased as the molecular weight was increased to about 100,000 Da but, minimal benefits were observed as the molecular weight was further increased [31].

(3) The *electronic theory* suggests that attractive forces between oppositely charged cationic delivery vehicles and the negatively charged mucin facilitates adhesion. This mechanism is dominant for cationic nanocarriers such as chitosan-based polymers, with mucoadhesion being particularly attributed to ionic interactions between the polymer and anionic sialic acid groups on the mucosal membrane [32, 33].

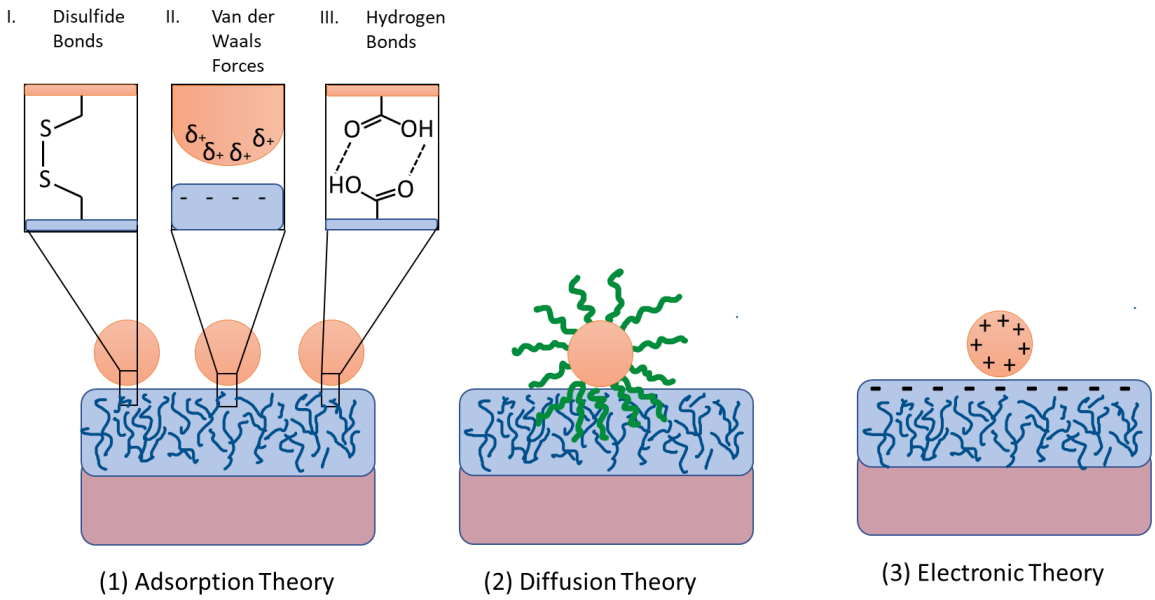

Figure 2. Mechanisms of mucoadhesion for ocular drug delivery vehicles.

Aside from these physical mechanisms, covalent bonding, or specific affinity interactions such as glycoconjugate-lectin interactions [34, 35] have been proposed to promote mucoadhesion. For example, thiolated polymers can form covalent bonds through disulfide bridges with cysteine units on mucin glycoproteins [36, 37], while phenylboronic acid modified nanocarriers can form reversible covalent complexes with 1,2-diols or 1,3-diols on mucin proteins [38, 39]. Many of these interactions are dependent on environmental factors such as the surrounding pH, temperature, water content and ionic strength, all of which can influence the conformation of mucin by influencing electrostatic expansion and repulsion of the mucin fibers, [10] and/or the strength of the mucoadhesive interactions to the polymer itself. For example, both thiolated polymers and phenylboronic acid modified nanocarriers form weaker interactions under more

acidic conditions [40]; in contrast, in the case of carboxylic acid-functionalized polymers such as poly(acrylic acid) (PAA), decreasing the pH of the surroundings promotes protonation of carboxyl functional groups which in turn leads to the formation of hydrogen bonds with mucin proteins that promote adhesion [41-43].

2.4. Mucoadhesive Nanocarriers

By leveraging the mechanisms of mucoadhesion, several types of mucoadhesive nanocarriers have been designed and reported for use in the eye.

2.4.1. Hydrogen-Bonding Nanocarriers

Mucoadhesive polymers containing functional groups capable of hydrogen bonding such as hydroxyl, carboxyl, amino, and sulfate functional groups can hydrogen bond with sugar residues of the ocular mucin [17]. Carboxylated polymers are particularly widely used in this regard. While at neutral pH, the negative charge of the carboxylated polymer is thought to electrostatically repel the negatively charged mucin-layer in the ocular microenvironment (pH~7.4 [44]), the local pH around such polymers, particularly when they are highly concentrated on the surface of a nanocarrier, can be significantly lower [18], thus promoting hydrogen bonding [10]. However, the highest adhesion strength between carboxylated polymers and mucin still occurs at lower pH values at which the carboxyl groups are at or below their pK_a values and therefore in the protonated form [45].

2.4.1.1. Hydrogen-Bonding Synthetic Polymers

Anionic synthetic polymers typically employed as mucoadhesive nanocarriers include PAA and its derivatives. PAA is historically the most widely studied mucoadhesive synthetic polymer, with its lightly crosslinked derivatives Carbopol® and Carbomer® having, in particular, been used extensively [10]. Incorporation of PAA into NPs also imparts mucoadhesive benefits. For example, PAA NPs synthesized by Bergey *et al.* showed no cytotoxicity to human corneal cells, high encapsulation efficiency (> 80%) of brimonidine, and effective *ex vivo* mucoadhesion [46]; similarly, El-Rahim *et al*. showed that poly(vinyl pyrrolidone) (PVP-PAA) nanogels prepared via the solution irradiation of acrylic acid monomer in the presence of pre-formed PVP polymer chains showed mucoadhesion (consistent with both components being strong hydrogen bonders) while also enabling controlled release of pilocarpine over 6 hours [47].

2.4.1.2. Hydrogen-Bonding Biopolymers

Hydrogen-bonding biopolymers typically employed for mucoadhesive nanocarriers include hyaluronic acid (HA), cellulose derivatives such as carboxymethylcellulose and hydroxypropyl methylcellulose [48], sodium alginate (SA) [49], and pectin [28]. The use of biopolymers as mucoadhesives provides benefits based on their inherent cytocompatibility, biodegradability, ocular tolerability, and, in some cases, the ability to enhance the ocular permeation of particles and thus drug payloads [5]. Such polymers are also commonly used in commercial eyedrop formulations, typically as lubricants; for example, Systane®

Ultra contains sodium hyaluronate and Kaiser Permanente Lubricant eye drops contain sodium carboxymethyl cellulose. As such, the adaptation of such polymers into the context of an ocular mucoadhesive delivery vehicle offers a minimal barrier to translation.

HA, a glycosaminoglycan, is naturally present in the vitreous body and the aqueous humor and has been investigated for its ability to act as a mucoadhesive and to improve the ocular permeability of the drug payload [50]. For example, coating micron-scale niosomes based on poloxamer 188, phosphatidylcholine and cholesterol with HA significantly improved the mucoadhesion of the niosomes, enabling the maintenance of higher precorneal concentrations of Tacrolimus (FK506), a hydrophobic drug pre-loaded inside the niosomes [51]. Other examples of HA-based particulate delivery systems include HA/chitosan particles [52, 53], HA/lipid particles [54], and gelatin particles with HA surface decoration [55], all of which improved ocular retention of the NP in the eye. Terreni *et al.* published results on a formulation of a variety of surfactants that, when coupled with HA, formed ~14 nm nano-micelles capable of encapsulating 0.105% (w/w) Cyclosporine-A (Cyc-A), a level ~ double the drug loading of the market staple ophthalmic Cyc-A emulsion Restasis® (0.05% w/w) and slightly higher than a competitor Ikervis® (0.1% w/w) [56]. The nano-micelles showed excellent mucoadhesive capability and slower release kinetics (up to 4 times slower than Ikervis®, a commercially available Cyc-A formulation), enabling enhanced precorneal residence times [56].

2.4.2. Cationic Nanocarriers

Mucoadhesion using cationic polymers is primarily attributed to electrostatic interactions between the cationic polymer and the anionic sialic acid residues in mucin; however, hydrogen bonding and polymer chain interpenetration can also contribute to the mucoadhesive properties of such polymers. Polymers are most generally made cationic via the presence of or incorporation of amino groups, whose pK_a (~9-10) lies above ocular pH, ensuring that the majority of the functional groups remain protonated in the tear film to promote electrostatic interactions with mucin.

Chitosan (CS) and its derivatives are the most widely explored cationic polymers used as mucoadhesives, although other polymers such as gelatin have also been proposed [57]. CS is a semi-synthetic polymer containing primary amine groups that is derived from the deacetylation of the biopolymer chitin and offers the advantages of being cytocompatible, biodegradable, through the action of lysozyme found in tear fluid, and tolerable *in vivo* [58]. CS has also the proven ability to loosen tight junctions between cells, imparting penetration enhancing properties through both the paracellular and intracellular routes [59]. The interactions between mucin and CS are reviewed in depth by Collado-Gonzalez *et al.* [60].

Nanocarriers of CS are often produced by the ionotropic gelation method using sodium tripolyphosphate (TPP) as a crosslinker and have been evaluated

recently for their effectiveness in the delivery of rosmarinic acid [61], lutein [62], dexamethasone [53, 63, 64], dorzolamide HCl [65], antibiotics [66, 67], timolol maleate [49], agomelatine [68], and erythropoietin [52]. While CS nanocarriers can be used on their own [61, 65], the majority of CS-based mucoadhesive drug delivery systems involve the use of a hybrid system. CS is often mixed with a high molecular weight anionic polymer such as PAA, HA, SA, pectin, and dextran (Dex) or dextrin derivatives [69]. In this case, the anionic polymer acts similarly to TPP as an ionic crosslinking agent for CS while also imparting additional mucoadhesive characteristics, improving the permeability of the nanocarriers, increasing drug retention, and decreasing burst release of drug [5].

2.4.3. Boronic Acid Nanocarriers

Boronic acids, and in particular phenylboronic acid (PBA), can form reversible covalent complexes of 5 and 6-membered boronate esters with *cis*-1,2 and/or 1,3 diols [70] in many monosaccharides and polysaccharides, including sialic acid residues in mucin. The charged form of the boronic acids is responsible for their high binding affinity with *cis*-diol groups; as such, the strength of the interaction between boronic acids and mucin is pH dependent. In the ocular tear film (pH~7.4), a simple 2-methyl-1-PBA moiety has a pK_a ~ 9.7 [71], resulting in relatively weak complexes with sialic acid. However, the degree of ionization and thus binding affinity can be tuned by the chemistry around the boronic acid group; for example, the acidity of different boronic acids can be described as aryl > alkyl such that the selection of PBA-based moieties is preferred over alkyl-based moieties [71].

Methods for modifying the PBA moiety to decrease the pK_a to ocular pH include the use of electron-withdrawing groups on nearby sites on the aryl ring [72] and the incorporation of the boronic acid in the ortho position to an amine [73], the latter enabling the formation of a cyclic N-B intramolecular interaction which lowers the pK_a of the boronic acid below neutral pH without any other modification of the aromatic group (Figure 3).

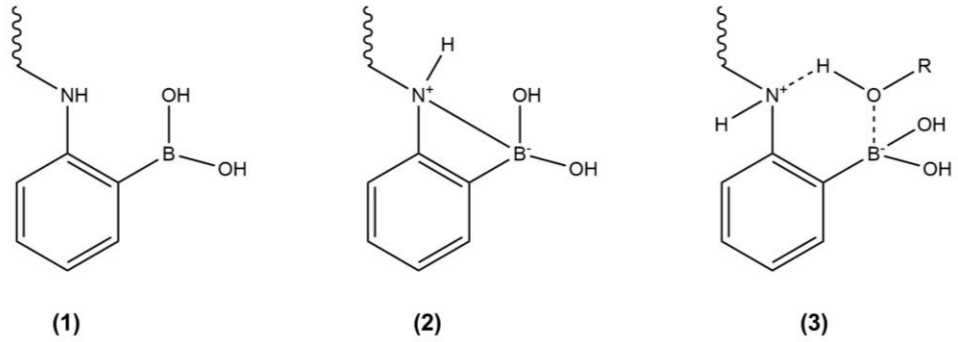

Figure 3. Phenylboronic acid containing amine group at ortho position to the boronic acid (1). Nitrogen-boron interaction (2), and solvent-inserted N-B interaction (3). R = H (water), CH_3 (methanol), or other protic solvent.

PBA-based NPs have been demonstrated to enhance mucoadhesion and thus drug delivery in the eye. In 2012, Liu *et al.* proposed a nano-micelle based on polylactic acid-*block*-dextran-*graft*-phenylboronic acid (PLA-*b*-Dex-*g*-PBA) polymers that facilitated sustained release of Cyc-A over a 5 day period at clinically relevant doses and was more mucoadhesive than the control PLA-*b*-Dex nano-micelles [74]. A follow-up study in 2016 compared the *in vivo* performance of the NP to the market staple Restasis® in a dry-eye induced mouse model using C57BL/6 mice, demonstrating the potential for 50 to 100-fold reduced dosing of

Cyc-A due to the improved retention of the nano-micelles and thus the potential for reduced toxicity and improved patient compliance; the 0.005 and 0.01% Cyc-A loaded NPs also enabled recovery of epithelial surface goblet cells over a 4 week trial while the 0.025% Cyc-A loaded NPs did not [43], hypothesized to be due to the elevated dose over an extended period of time slowing or preventing the recovery of the ocular surface. Prosperi-Porta *et al.* designed a polylactic acid-*block*-methacrylic acid-*co*-3-(acrylamido)phenylboronic acid (PLA-*b*-P(MAA-*co*-3-AAPBA)) nano-micelle with interesting polymerization kinetics that resulted in a gradient of MAA to 3-AAPBA radially outwards within the hydrophilic block. These nano-micelles were more mucoadhesive than CS and non-PBA controls, enabled higher Cyc-A loading (15 wt % Cyc-A/polymer compared to 12 wt % Cyc-A/polymer achieved by Liu *et al.*), and achieved improved delivery of Cyc-A compared to Restasis® [39]. More recently, Tan *et al.* designed nanostructured lipid carriers (NLC) loaded with dexamethasone and surface functionalized with (3-aminomethyl)phenylboronic acid-conjugated chondroitin sulfate that exhibited similarly enhanced ocular residence time, mucoadhesion, and drug release kinetics compared to dexamethasone-loaded NLC controls [75].

2.4.4. Thiolated Nanocarriers

The next generation of mucoadhesive nanocarriers is being designed to covalently adhere to the ocular mucin. The protein backbone of mucin contains large cysteine repeat domains, meaning there exist many free thiols in addition to disulfide bonds within and between mucin strands that aid in forming the mesh

network that is a mucin gel [15]. Thiolated nanocarriers can thus form disulfide bonds through oxidation with the free thiols within the mucin and/or disulfide bonds through a thiol-disulfide exchange reaction with existing disulfide bonds present within and between the mucin strands. The reversibility of disulfide bonds is thought to result in a combination of initial mucoadhesion and, in some cases, ultimate mucopenetration as thiolated nanocarriers actively cleave disulfide bonds present between mucin strands, allowing the nanocarriers to diffuse to the epithelial surface [10]; once there, thiolated nanocarriers can also act as permeation enhancers by reducing the oxidized glutathione released by cells that can then inhibit protein tyrosine phosphatase from closing tight cell junctions [76].

Many common mucoadhesive polymers such as CS and PAA have been modified through thiolation (commonly referred to as thiomers [77]), leading to markedly improved mucoadhesive properties. Zhu *et al.* produced thiolated CS/SA NPs that showed improved mucoadhesion based on zeta-potential measurements, enabling higher levels of fluorescein to be delivered to rabbit corneas compared to the control CS/SA NPs [78]. Li *et al.* compared the mucoadhesive properties of N-acetyl cysteine-modified chitosan (CS-NAC) to those of chitosan oligosaccharide and carboxymethyl chitosan surface-modified curcumin loaded NLC (CUR-NLC) [79]. The highest mucoadhesion and the most sustained release profile was observed with the CS-NAC-CUR-NLC, which enabled a release of just under 40% of loaded curcumin over 72 hours with minimal burst release. Furthermore, the CS-NAC modified NLCs had a significantly larger

steady state flux (J_{ss}) and apparent drug permeation (P_{app}) than all other formulations over the entirety of the 6-hour measurement time, demonstrating the effectiveness of the particle as a permeation enhancer for ocular drug delivery [79]. Thiolated NPs based on poly(aspartic acid) [80] and PEG [81] have also been shown to have similar benefits.

2.5. Preactivated Thiomers

While thiomers have shown exceptional mucoadhesive properties and the potential for treatment of diseases such as dry eye disease (DED) [82], there exist roadblocks to their use in eye drop formulations. Thiomers have the unfortunate property of being unstable and prone to oxidization of their thiols at pH ≥ 5 [83]. The optimal pH of instilled therapeutics would mimic that of the ocular tear film (pH ~ 7.4) and as the pH moves further away from this value, the instilled therapeutic can lead to patient discomfort [84]. Therefore, thiomers are not an ideal form of treatment for topically instilled therapeutics. However, recent advancements in the field of mucoadhesion have brought about a new generation of mucoadhesives which may offer a solution to the problem of thiomer oxidation.

The term *preactived thiomer* was coined by the Bernkop-Schnurch lab from the University of Innsbruck [85]. The idea of a preactived thiomer is one in which the thiol present in a thiomer is preactivated by the formation of a disulfide ligand (Figure 4). The concept was adapted from previous knowledge in covalent chromatography where molecules containing cysteine residues are effectively

covalently bound to thiol bearing ligands, that are preactivated with a pyridyl group, through a thiol/disulfide exchange reaction releasing the 2-pyridinethione ligand which can be observed by spectroscopy at λ = 343 nm (Figure 5) [83, 86]. The properties of the pyridyl disulfide (PDS) group are such that when the tertiary amine becomes protonated, the disulfide bond is activated and the 2-pyridinethione becomes a superior leaving group [86]. Due to the relatively low pK_a of the tertiary amine of pyridine (~ 5.3) the reaction between a polymer containing PDS and a thiol ligand can be performed under acidic conditions, which also aids in preventing self-oxidation of the thiol reagent in solution [86]. A benefit to using PDS in thiol-disulfide exchange reactions is that the subsequent 2-pyridinethione group is a more stable molecule that will not participate in subsequent thiol/disulfide exchanges, allowing for nearly 100% efficiency in modification [86].

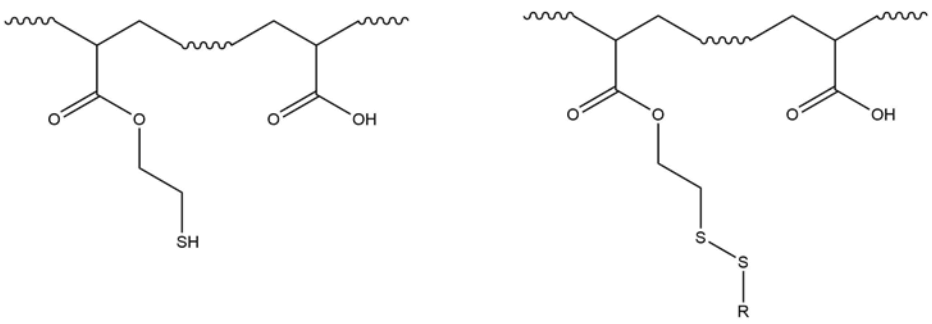

Figure 4. Example of a thiomer (left) and a preactivated thiomer (right). R = a thiolated ligand.

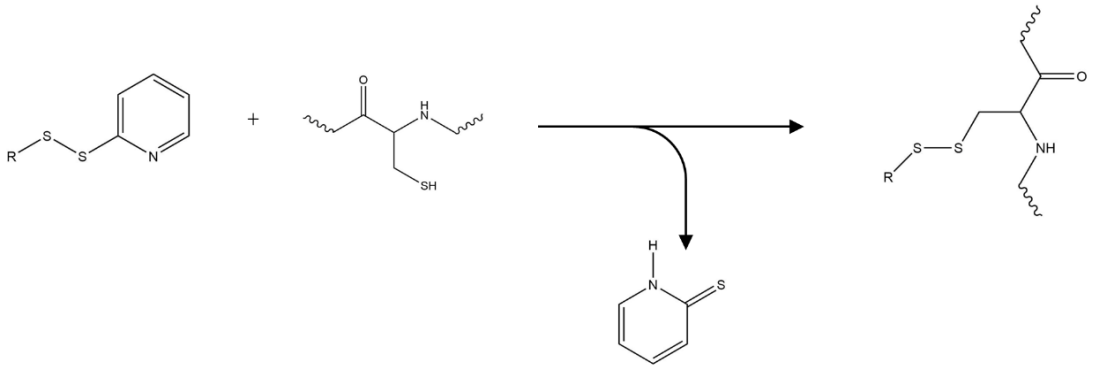

Figure 5. Covalent chromatography with PDS group forms covalent interactions with molecules containing free thiols in cysteine residues. Thiol/disulfide exchange reaction results in leaving group 2-pyridinethione (λ = 343 nm). R = chromatography resin.

PDS has been shown to react very rapidly with thiols, however the resultant 2-pyridinethione leaving group is toxic and therefore to use this concept in their research, the Bernkop-Schnurch lab formulated an alternative leaving group that maintained the high reactivity of the pyridyl group, while removing concerns over toxicity. With the incorporation of 2-mercaptonicotinic acid (2-MNA) into preactivated thiomers, they were able to solve the problem of oxidation experienced with thiomers and the toxicity concerns of the 2-pyridinethione leaving group [85]. The preactivated thiomer achieves mucoadhesion in a similar way to thiomers, namely through a thiol/disulfide exchange reaction with cysteine-rich subdomains of mucin. Through their work, Bernkop-Schnurch *et al*. were able to achieve significantly stronger mucoadhesive properties from their poly(acrylic-acid)-cysteine-2-MNA (PAA-cys-2-MNA) preactivated thiomer formulation compared to their PAA-cys thiomer control [85]. This initial work led to many follow

up studies on the preactivated thiomer modification of mucoadhesive polymers such as CS [87], pectin [88], and HA [89]. Further work by the group investigated the use of preactivated thiomers in NPs, showing similar improvements in mucoadhesion compared to controls [37].

In a recent study, a comparison was performed between highly reactive pyridyl based ligands and less reactive thiol ligands in preactivated thiomers [90]. This study found that by incorporating less reactive thiol ligands such as NAC in place of pyridyl ligands into preactived thiomers, mucoadhesion was improved [90]. In rheological studies, the group found that the viscosity of their PAA-cys-NAC/mucin sample was significantly ($p < .05$) higher (10.9 fold) than their PAA-cys-2-MNA/mucin sample (5.6 fold) when compared with controls [90]. The hypothesis for the improved mucoadhesion was that the highly reactive pyridyl ligands were reacting immediately upon contact with mucin, preventing penetration into the mucin gel required for the prolonged contact time of the material [90]. In contrast, the less reactive thiol ligand NAC allowed for initial penetration of polymer chains into the mucin-layer prior to forming a covalent bond with the mucin, allowing for stronger adhesion [90].

Based on the promising results of this prior research the use of preactivated thiomers to create novel mucoadhesive micelles is investigated in the current work and the results with these preactivated thiomer mucoadhesives are compared to those previously obtained using PBA as the mucoadhesive component [39].

Polymeric micelles were chosen as the delivery vehicle based on the ability to encapsulate large amounts of hydrophobic drug in their core, and the high degree of water solubility imparted by their hydrophilic corona [91]. The high degree of functionality of polymers also allows us to test many different organic mucoadhesive chemistries. The ease of scale-up and low cost of production in comparison to other nanocarriers makes them an attractive option [91].

3. MATERIALS & METHODS

3.1. Materials

All chemicals and solvents were purchased from Sigma-Aldrich (Oakville, Ontario) and used as obtained, unless otherwise specified. 3-(acrylamido)phenylboronic acid (98%; 3-AAPBA) was purchased from Sigma-Aldrich and purified by recrystallization in purified water prior to use. Azobis(isobutyronitrile) (AIBN) was purified by recrystallization in methanol (MeOH). Poly(D,L-lactide), 4-cyano-4-[(dodecylsulfanylthiocarbonyl)sulfanyl]pentonate with molecular weight 5 kDa (PLA-CDP) was purchased from Sigma-Aldrich. Purified water with a resistivity of 18.2 MΩ cm was prepared using a Milli-pore Barnstead water purification system (Graham, NC, USA). Phosphate buffered saline (PBS 10X, 1M, pH 7.4) was purchased from BioShop (Burlington, ON) and diluted 10x to obtain a 0.1M (1X) solution with purified water prior to use. Monobasic sodium phosphate monohydrate ($NaH_2PO4 \bullet H_2O$) and dibasic sodium phosphate heptahydrate ($Na_2HPO_4 \bullet 7H_2O$) were purchased from EMD Chemicals (Darmstadt, Germany) and used to make a 10 mM sodium phosphate buffer in purified water. Regenerated cellulose dialysis membranes with a molecular weight cut off (MWCO) of either 3.5 or 6-8 kDa were purchased from Spectrum Laboratories Inc. (Rancho Dominguez, CA, USA). EZFlow® 13 mm high pressure liquid chromatography (HPLC) grade nylon syringe filters with 0.45 and 0.2 µm pore sizes were purchased from Foxx Life Sciences (New Hampshire, USA).

3.2. Monomer Synthesis

The synthesis of the monomer pyridyl disulfide ethyl methacrylate (PDSMA) involved an intermediate product, pyridyl disulfide alcohol (PDSOH) which was synthesized and purified according to a modified literature source [92]. Aldrithiol-2 (1.250 g, 5.65 mmol; 1 eq.) was dissolved in 15.0 mL of MeOH and stirred at constant speed. Glacial acetic acid (2.5 mL, 43.70 mmol; 7.7 eq.) was added to the stirring solution dropwise using an addition funnel. A solution of β-mercaptoethanol (0.3 mL, 4.30 mmol; 0.72 eq.) in MeOH (10.0 mL) was prepared and added dropwise to the stirring solution using the addition funnel. The reaction was left stirring at room temperature for 24 hours. Solvent volume was reduced using rotary evaporation and the crude product was redissolved in 25.0 mL of dichloromethane (DCM). Extractions were performed against saturated $NaHCO_3$ (2 x 25 mL), purified water (1 x 25 mL) and saturated brine (360 g/L of NaCl in purified water; 1 x 25 mL). The organic phase was then dried with $MgSO_4$ and gravity filtered. Solvent volume was reduced using rotary evaporation, resulting in final product, a yellow oil. Subsequently, silica column chromatography was used for purification (2:3 Hexanes/Ethyl Acetate (EtOAc)) where PDSOH had an R_f ~ 0.5 from thin layer chromatography (TLC) in these solvents. The collected samples of PDSOH were combined and the solvent volume reduced by rotary evaporation, to obtain the final product as a yellow oil (52.7% yield). Successful synthesis was determined by proton nuclear magnetic resonance (^{1}H NMR; Bruker AV 600 MHz). ^{1}H NMR in deuterated chloroform ($CDCl_3$): δ [ppm] = 8.51 (pyridine proton *ortho*-

N), 7.58 (pyridine proton *para*-N), 7.40 (pyridine proton *ortho*-disulfide), 7.15 (pyridine proton *meta*-N), 5.68 ($CH_2CH_2O\boldsymbol{H}$), 3.80 ($CH_2C\boldsymbol{H_2}OH$), 2.95 ($C\boldsymbol{H_2}CH_2OH$).

PDSMA, synthesized by reaction of PDSOH with methacryloyl chloride, was prepared based on a modified literature protocol [92]. PDSOH (0.564 g, 3.01 mmol; 1 eq.) was dissolved in anhydrous DCM (10.0 mL). *N,N*-Diisopropylethylamine (DIPEA) (1.05 mL, 6.02 mmol; 2 eq.) was added dropwise to the stirring solution, which was then placed in an ice bath to cool to 0°C. A solution of methacryloyl chloride (0.38 mL, 3.91 mmol; 1.3 eq.) in anhydrous DCM (10.0 mL) was then added dropwise to the stirring reaction over 30 minutes by an addition funnel. The reaction was stirred at constant speed for 24 hours and then allowed warm to room temperature. The colour of solution changed from yellow to dark brown overnight. The solution was then transferred to a separatory funnel and extractions were run against 1M HCl (1 x 20 mL), 1M NaOH (1 x 20 mL), PBS (1X, 0.1M, pH 7.4; 1 x 20 mL), and a saturated brine wash (360 g/L of NaCl in purified water; 1 x 20 mL), followed by drying with $MgSO_4$, gravity filtering, and solvent volume reduction by rotary evaporation. The crude product was a yellow oil which was purified by silica column chromatography (3:1 Hexanes/EtOAc). The final product had an R_f ~ 0.3 from TLC in these solvents. PDSMA column samples were collected, and the volume reduced with rotary evaporation to obtain final product as a yellow oil (49.5% yield). ^{1}H NMR (Bruker AV 600 MHz; $CDCl_3$) showed the following: δ [ppm] = 8.47 (pyridine proton *ortho*-N), 7.68 (pyridine proton *para*-N), 7.63 (pyridine

proton *ortho*-disulfide), 7.09 (pyridine proton *meta*-N), 6.12 (vinylic proton, *cis*-ester), 5.58 (vinylic proton, *trans*-ester), 4.40 ($SCH_2C\boldsymbol{H_2}O$), 3.09 ($SC\boldsymbol{H_2}CH_2O$), 1.94 ($CCH_2C\boldsymbol{H_3}$).

3.3. Nano-micelle Synthesis

3.3.1. Gel Permeation Chromatography (GPC)

To characterize the molecular weight (MW) of the purchased PLA-CDP, gel permeation chromatography (GPC) was employed. GPC (Polymer Laboratories) was run using three installed Phenomenex Phenogel™ columns (300 x 4.6 mm, 5 µm; pore sizes: 100, 500, 10^4 Å) at room temperature and the molecular weight compared to that obtained using a calibration curve generated using linear PEG standards (Polymer Laboratories). PLA-CDP was dissolved in dimethyl formamide doped with 50 mM LiBr and run with the same solvent as the eluent. Samples were filtered through 0.2 µm Teflon pore syringe filters prior to injection.

3.3.2. Reversible Addition-Fragmentation Chain-Transfer (RAFT) Polymer Synthesis

Polymers produced herein were prepared using the same molar feed ratios as in previous work, the only difference being an exchange of the mucoadhesive monomer component depending on the polymer to be made. Poly(D,L-lactide-*block*-(methacrylic acid-*co*-pyridyl disulfide ethyl methacrylate)) or LMS, and Poly(D,L-lactide-*block*-(methacrylic acid-*co*-3-(acrylamido)phenylboronic acid)) or LMP, were synthesized using reversible addition-fragmentation chain-transfer

(RAFT) polymerization. The use of PLA for the hydrophobic segment stems from its history of being used in biomedical applications, including micelles, and its long-standing FDA approval [93]. Methacrylic acid (MAA) was passed through a column packed with inhibitor remover beads. For synthesis of LMS and LMP, the method proposed by Prosperi-Porta *et al.* was used to make polymers with a feed ratio of 80:20:1.4:0.2 (MAA/(PDSMA or 3-AAPBA)/PLA-CDP/AIBN respectively) [39]. These polymers were designated LMS-20 and LMP-20 in accordance with previous terminology (20 mol % PDSMA or 3-AAPBA in the hydrophilic block) [39]. MAA (300 mg, 3.49 mmol), 3-AAPBA (166.4 mg, 0.87 mmol) or PDSMA (222.5 mg, 0.87 mmol), PLA-CDP (312 mg, 0.061 mmol), and AIBN (1.43 mg, 0.0087 mmol) were mixed with 7.8 mL of 9:1 dioxane/water (% v/v) to make a 10 % (w/v) solution in a 25 mL round-bottom flask. The reaction mixture was purged with nitrogen for 30 minutes, then heated in an oil bath to 70°C for 24 hours with constant stirring. The solvent volume was then reduced by rotary evaporation and the copolymers were redissolved in THF and isolated by precipitation into 10 times excess cold anhydrous diethyl ether (3 x 250 mL) with filtration through a Büchner funnel apparatus. The copolymer was left partially covered in the fume hood to dry for 48 hours. The molecular weight and composition of the copolymers were determined by ^{1}H NMR (Bruker AV 600 MHz) in deuterated dimethyl sulfoxide (DMSO-d_6).

3.3.3. Post-Polymerization Modification

To produce the final versions of the LMS-20 polymer, a post-polymerization modification was performed with small thiol molecules through a thiol/disulfide exchange reaction, based on a protocol modified from the one proposed by Peng *et al.* [94]. In a typical reaction procedure, 30 mg of LMS-20 polymer (20.6 kDa, 1.69 x 10^{-3} mmol) was dissolved in 6 mL of acetone to make a 5 mg/mL solution. A small amount of glacial acetic acid (~ 3 drops) was added to ensure an acidic environment to improve reaction kinetics and prevent thiol oxidation. The small thiol molecule of choice; either Cysteamine (Cys), Glutathione (GSH), or *N*-acetyl cysteine (NAC), was dissolved separately in a suitable solvent (acetone for NAC; purified water for Cys & GSH) to a concentration of 50 mg/mL. From this stock solution, a volume was transferred to the polymer solution such that the molar ratio of thiol to pyridyl group was 3:2 (i.e., 5.4 mg or 0.0696 mmol of Cys, 21.4 mg or 0.0696 mmol of GSH, 11.36 mg or 0.0696 mmol of NAC). The reaction was left to stir at room temperature overnight. Each reaction mixture was then transferred to Spectra/Por® 3.5 kDa MWCO regenerated cellulose dialysis tube and dialyzed against purified water for 4 days, with periodic changes of the water. Subsequently, dialyzed polymer was transferred to 20 mL glass vials, frozen, and lyophilized over 2 days to obtain the final product, a yellow powder. The composition of the modified copolymers was determined by ^{1}H NMR (Bruker AV 600 MHz) in DMSO-d_6 and/or deuterated water (D_2O). The final copolymers were named LMC-20, LMG-20, and LMA-20 for Cys, GSH, and NAC modified LMS-20 respectively.

3.3.4. Polymer Nanoprecipitation

To form nano-micelles out of the synthesized polymers, the polymer of choice was dissolved in acetone to a concentration of 20 mg/mL, then heated in an oven to 50°C for 5 minutes. To this polymer solution was added 3-5 drops of 10 mM sodium phosphate buffer and the mixture reheated in the oven at 50°C. The process was repeated until it resulted in a clear solution.

The polymer solution was then added dropwise (~ 1 drop/s) through an 18G needle into a stirring solution of 10 mM sodium phosphate buffer (pH 7.4). The mixture was covered with an aluminum tent to allow acetone evaporation and left stirring at 850 RPM for 48 hours. Final nano-micelle solutions of 10 mg/mL resulted, and were pH adjusted to 7.4 and filtered through 0.45 µm pore nylon syringe filters prior to use, overwise stored in the fridge at 4°C.

Drug-loaded micelles were prepared in a similar manner. Cyc-A was dissolved in acetone to a concentration of 5 mg/mL and from this solution the desired amount of drug was transferred to the polymer solution described above. Subsequently, the polymer/drug mixture was added dropwise to 10 mM sodium phosphate buffer, or PBS (0.1M, pH 7.4; drug release and rheological studies), in the same manner.

3.4. Nano-micelle Characterization

3.4.1. Size Determination

The particle size of LMA-20 and LMP-20 nano-micelles was determined using DLS using a Brookhaven 90 Plus Particle Size Analyzer to get the average

effective diameter and polydispersity index (PDI) of the nano-micelles. 2 mL of nano-micelle solution in 10 mM sodium phosphate buffer at a concentration of 1 mg/mL and pH 7.4 was added to a polystyrene two transparent sided cuvette, a concentration chosen to obtain the appropriate count rate.

3.4.2. Morphology

The shape and structure of the LMA-20 and LMP-20 nano-micelles was observed by Transmission Electron Microscopy (TEM). A Jeol TEM-1200EX transmission electron microscope with an 80 kV electron beam was used. TEM samples were prepared by air-drying 2 µl of 1 mg/mL micelle solution in 10 mM sodium phosphate at pH 7.4 on a carbon coated 400 mesh copper grid prior to analysis. Samples were measured at a level of magnification of 50000.

3.4.3. Critical Micelle Concentration

The Critical Micelle Concentration (CMC) was determined through the pyrene fluorescence method [95]. A stock solution of pyrene in acetone (100 µg/mL) was prepared and 4 µL transferred to 4 mL glass vials, allowing the acetone to evaporate overnight to form a pyrene film. Solutions of LMA-20 micelles in PBS (0.1M, pH 7.4) were prepared in a range of concentrations (10^{-6} mg/mL to 1 mg/mL) by dilution from a 10 mg/mL stock solution. 1 mL of each concentration was added to each glass vial containing pyrene. Mixtures were shaken for 24 hours, then analyzed using a BioTek Cytation 5 Cell Imaging Multi-Mode Reader in fluorescence intensity mode (Vermont, USA) with an excitation wavelength of

340 nm and emission wavelengths of 373 and 383 nm, with bandwidth of 9 nm. To determine the CMC, the fluorescence intensity ratio (I_{373}/I_{383}) as a function of the concentration of polymer was plotted, with the concentration plotted on a logarithmic scale.

3.4.4. Mucoadhesion (Zeta-Potential)

LMP-20 and LMA-20 micelle samples were prepared using the methods described in Section 3.3.3. A stock solution of porcine stomach mucin (PSM) Type III (Sigma Aldrich) at 10 mg/mL in 10 mM sodium phosphate salt (pH 7.4) was prepared and left stirring for 24 hours. Control samples of micelle and PSM were diluted to 5 mg/mL prior to incubation and analysis. A 1:1 mixture (v/v) of 10 mg/mL micelle solution and 10 mg/mL PSM was prepared to a final concentration of 5 mg/mL. Samples were placed in an incubating shaker at 37°C for 1.5 hours to allow for particle interactions prior to analysis. Samples were then placed into polystyrene two-sided cuvettes, and an AQ 1204 probe was placed into the cuvette. Samples were analyzed using the zeta-potential function on the Brookhaven 90 Plus Particle Size Analyzer at 25°C.

3.4.5. Mucoadhesion (Rheology)

Mucoadhesive properties of LMA-20 and LMP-20 were further compared through rheological measurements on a TA Instruments (Delaware, USA) discovery hybrid rheometer (DHR; Discovery HR-20), equipped with a C20/1° cone and Peltier plate combination, running TRIOS software. Measurements of complex

viscosity were made at angular frequencies from 0.1 to 100 s^{-1} and a strain of 1% at 15 °C.

Samples of LMA-20 and LMP-20 micelles at 10 mg/mL in PBS (0.1M, pH 7.4) were made in triplicate as described in Section 3.3.3. A 50 mg/mL mucin stock solution was prepared in PBS (0.1M, pH 7.4). Mixtures of micelle and mucin were prepared in triplicate by mixing micelle and mucin solutions 1:1 (v/v) and were incubated at 37°C overnight in an incubating shaker, while controls of micelles and mucin were prepared by mixing 1:1 (v/v) with PBS (0.1M, pH 7.4).

Rheological synergism was calculated to determine the extent of interaction between mucin and micelles through the following formula:

$$\Delta G' = G'_{mix} - (G'_{micelles} + G'_{mucin})$$

where G'_{mix} is the storage modulus (mPa) of the micelle/mucin mixture, $G'_{micelles}$ is the storage modulus (mPa) of the micelle control, and G'_{mucin} is the storage modulus (mPa) of the mucin control, all at an intermediate angular frequency of 10 s^{-1} [96].

3.5. Drug Release Studies

3.5.1. Drug Entrapment Efficiency (EE) & Drug Loading (DL)

Cyc-A loaded LMA-20 nano-micelles were synthesized as described. LMA-20 nano-micelle samples at a polymer concentration of 10 mg/mL and Cyc-A concentration of 1.5 mg/mL were obtained in PBS (0.1M, pH 7.4). A small sample

of each was taken for EE and DL studies. Briefly, micelle sample was transferred to an Eppendorf tube and centrifuged at 5000 RPM for 30 minutes. The supernatant was then diluted 100x in a separate Eppendorf tube with acetonitrile (ACN), representing the entrapped drug sample. The precipitate was mixed with 1 mL of ACN to make up the free drug sample and a sample made up diluted 100x. Samples were then filtered through 0.2 µm pore nylon syringe filters, transferred to 200 µl disposable inserts in 1 mL HPLC vials and run on an Agilent 1260 Infinity II HPLC utilizing a binary HPLC pump, autosampler, UV/Visible detector set to a wavelength of 210 nm, with an ACN/Water (80:20 v/v) mobile phase flowing at 0.7 mL/min through a Phenomenex C18 (150 x 4.6 mm, 5 µm particle size) column. Column temperature was set at 60°C, injection volume to 20 µl. The concentration of the samples was determined by generating a standard calibration curve of Cyc-A in the mobile phase.

3.5.2. Cyc-A Release Studies

Remaining Cyc-A loaded LMA-20 micelle samples from Section 3.5.1 were used for the release studies. 250 µL of each micelle sample was transferred to Spectra/Por® 6-8 kDa MWCO regenerated cellulose dialysis tubing and placed in ~ 7 x sink conditions of PBS (0.1M, pH 7.4), i.e., 100 mL for 1.5 mg/mL Cyc-A loaded micelles, at 37°C in an incubating shaker (100 RPM). Release samples of 10 mL were taken at intervals of 1, 3, 10 hours, 1, 2, 3, 7, and 10 days. Collected samples were frozen and lyophilized, then reconstituted in ACN/water (80:20, v/v) and concentrated five-fold. Samples were then shaken for 1 hour to phase

separate the salt and organic phase and extract the drug into the ACN. The organic phase of samples was filtered through 0.2 µm pore nylon syringe filters into Eppendorf tubes and stored at 4°C until further use. Release samples were transferred to 200 µl disposable inserts in 1 mL HPLC vials and run on HPLC as described above using the same instrument and methods from Section 3.5.1.

3.6. Statistical Analysis

To test for significance in the results, Minitab 18 was used to run a one-way analysis-of-variance (ANOVA), with a post-hoc Tukey's test, or Welch's test to account for unequal variances, to obtain *p*-values. The level $p < .05$ was set for significance, $p < .01$ for very significant, $p < .001$ for highly significant

4. RESULTS & DISCUSSION

4.1. Monomer Synthesis

Several attempts were made at synthesizing an appropriate preactivated thiol monomer. Two distinct methods were tried, which will be abbreviated as the Monomer from Scratch (MFS) and the Post-Polymerization Modification (PPM) methods.

In the MFS method, synthesis of the final version of monomers that would appear in the polymer were attempted. The benefit of this method is that these monomers could then be incorporated directly into the polymer during polymerization and the resulting polymer would require no further modification. Synthesis of the monomers in Figure 6 was performed.

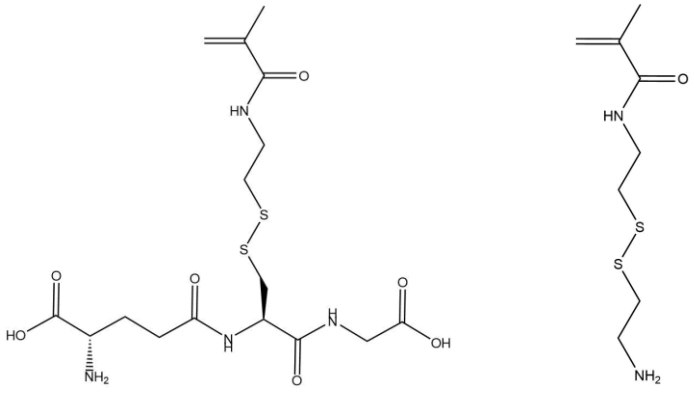

Figure 6. Chemical structures of Glutathione Disulfide Ethyl Methacrylamide (GDSMA; left) and N-Methacryloyl Cystamine (MAC; right).

The materials, methods, and results for the synthesis of both GDSMA and MAC can be found in Appendix A. However, attempts at the synthesis of these

monomers were either unsuccessful or required an impractical number of synthetic steps.

The PPM method involves the synthesis of a precursor monomer which could be incorporated into the polymer during polymerization, with the capability for subsequent modification via a thiol/disulfide exchange reaction. This method is commonly employed in the literature with the monomer PDSMA to introduce thiolated ligands into a polymer [86]. Due to the properties of the PDS group described in Section 2.5, the PDSMA monomer was chosen for the PPM method.

The reaction schemes for synthesis of the precursor PDSOH and PDSMA are presented in Figure 7 and Figure 8. The monomer precursor PDSOH and the monomer PDSMA were successfully synthesized, and results are shown in the ^{1}H NMR spectrums in Figure 9 and Figure 10 respectively and the results agree with literature for chemical shift [92].

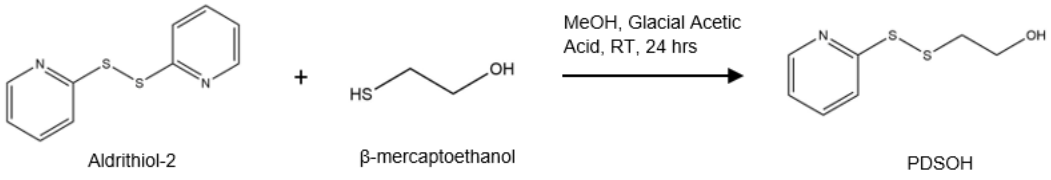

Figure 7. Reaction scheme for synthesis of PDSOH. Thiol/disulfide exchange reaction between aldrithiol-2 and β-mercaptoethanol yields PDSOH and is subsequently purified by column chromatography.

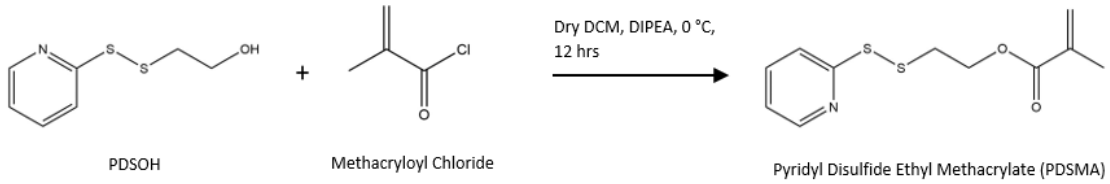

Figure 8. Reaction scheme for synthesis of PDSMA. Acyl chloride reaction of PDSOH with methacryloyl chloride is subsequently purified by column chromatography.

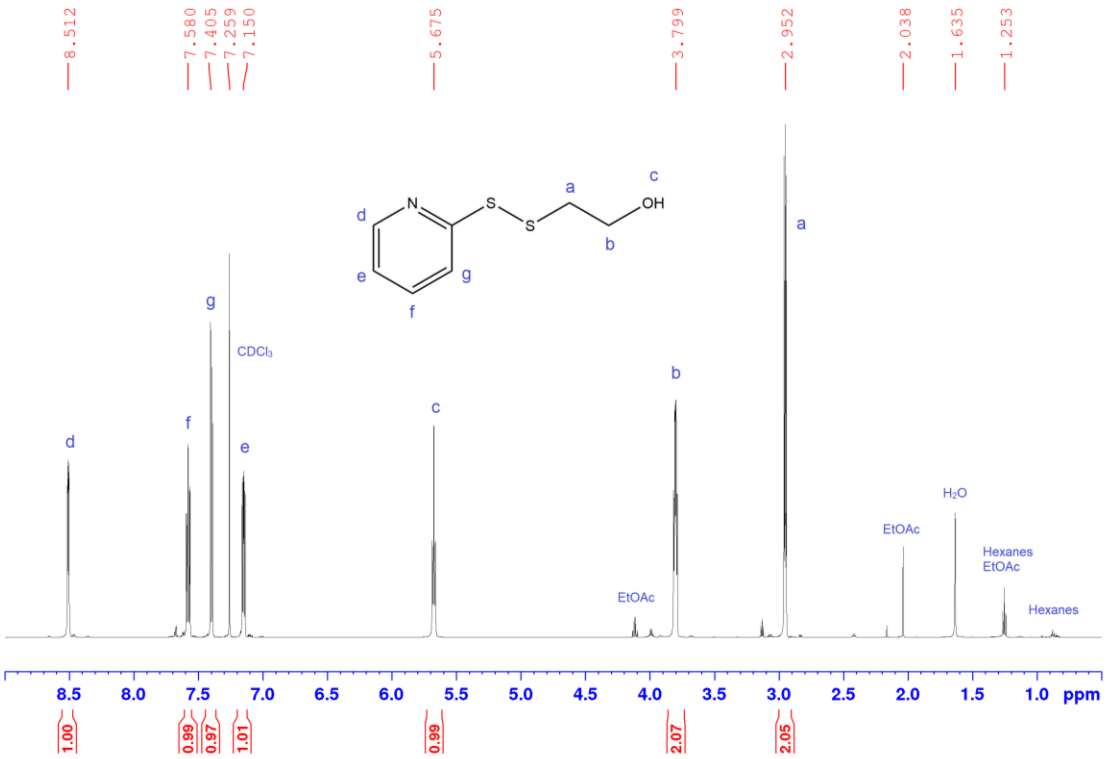

Figure 9. ^{1}H NMR spectrum of purified PDSOH product in $CDCl_3$. δ [ppm] = 8.51 (pyridine proton *ortho*-N), 7.58 (pyridine proton *para*-N), 7.40 (pyridine proton *ortho*-disulfide), 7.15 (pyridine proton *meta*-N), 5.68 ($CH_2CH_2O\boldsymbol{H}$), 3.80 ($CH_2C\boldsymbol{H_2}OH$), 2.95 ($C\boldsymbol{H_2}CH_2OH$).

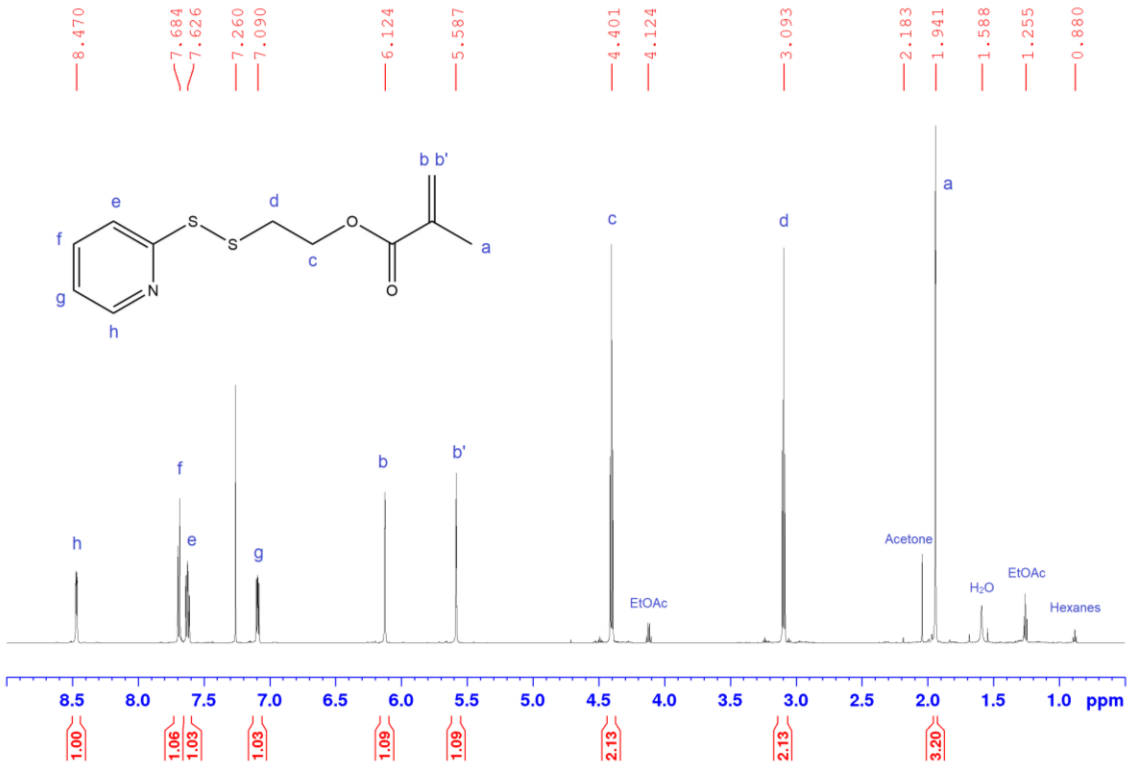

Figure 10. ^{1}H NMR spectrum of purified PDSMA product in $CDCl_3$. δ [ppm] = 6.1, 5.9 attributed to the introduction of the acrylate group and δ [ppm] = 1.95 indicative of the methyl group correspond to successful monomer synthesis.

The reaction yields from the PDSOH and PDSMA synthesis were 52.7% and 49.5% respectively. Previously, a 72% yield was reported, which is significantly higher than what was achieved in this work [92]. However, optimization of the reaction conditions as well as extraction protocols and purification may lead to improved yields.

4.2. Nano-micelle Synthesis

4.2.1. RAFT Polymer Synthesis

The synthesis of amphiphilic block copolymers using the RAFT polymerization technique has been used extensively in the literature [97]. Based on previous work in the Sheardown Lab, the polymers LMP-20 and LMS-20 were successfully synthesized using the RAFT polymerization technique [39]. The desire was to synthesize both polymers to investigate the mucoadhesive properties imparted by the PBA and preactivated thiomer moieties. The chemical composition and MW were characterized using ^{1}H NMR and the spectra for LMP-20 and LMS-20 can be seen in Figure 11 and Figure 12 respectively. Successful polymer synthesis was characterized by an elimination of acrylate peaks at δ ~ 6.0 – 5.5 and introduction of methyl and ethyl peaks from the polymer backbone at δ ~ 2.0 – 0.5.

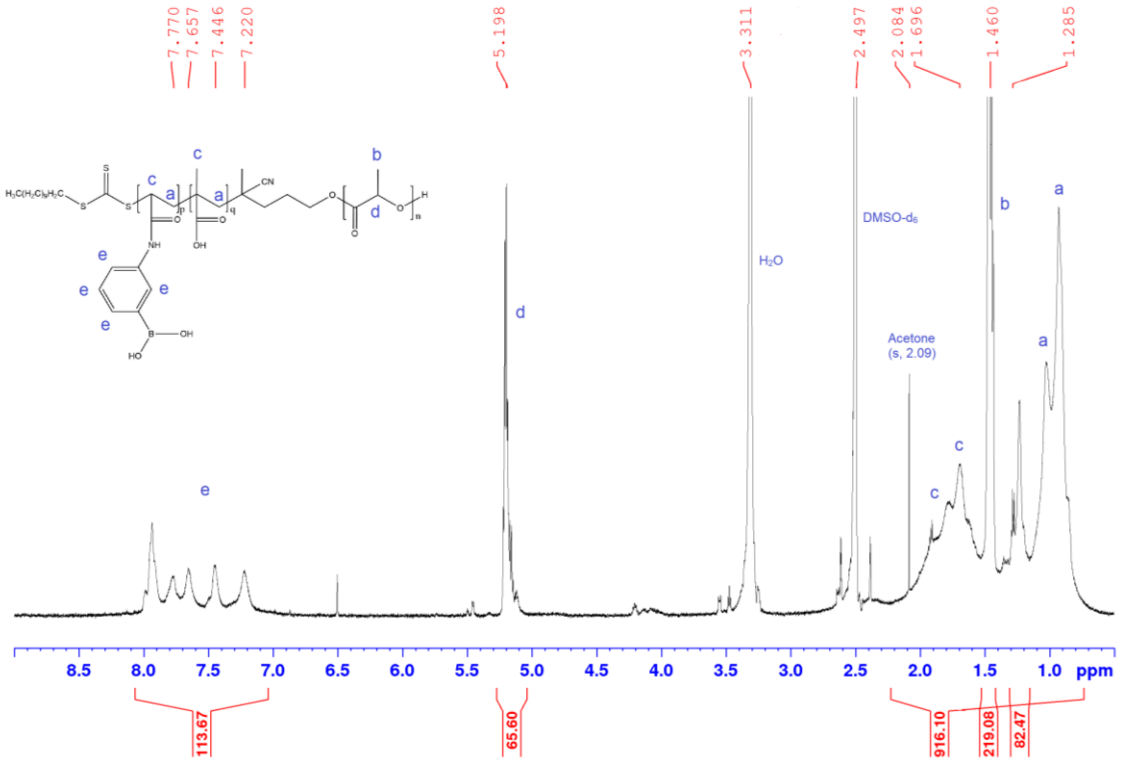

Figure 11. ^{1}H NMR spectrum of the LMP-20 polymer in DMSO-d_6. Elimination of acrylate peaks from δ [ppm] = 6.0 – 5.5 and introduction of methyl and ethyl peaks from polymer backbone at δ [ppm] = 2.0 – 0.5 indicate successful polymer synthesis. δ [ppm] = 8.0 – 7.0 (aromatic of 3-AAPBA), 5.2 (C***H*** of lactide), 2.0 – 0.5 (methyl and ethyl peaks of MAA), 2.0 – 0.5 (ethyl peaks associated with 3-AAPBA), 1.45 (methyl of lactide).

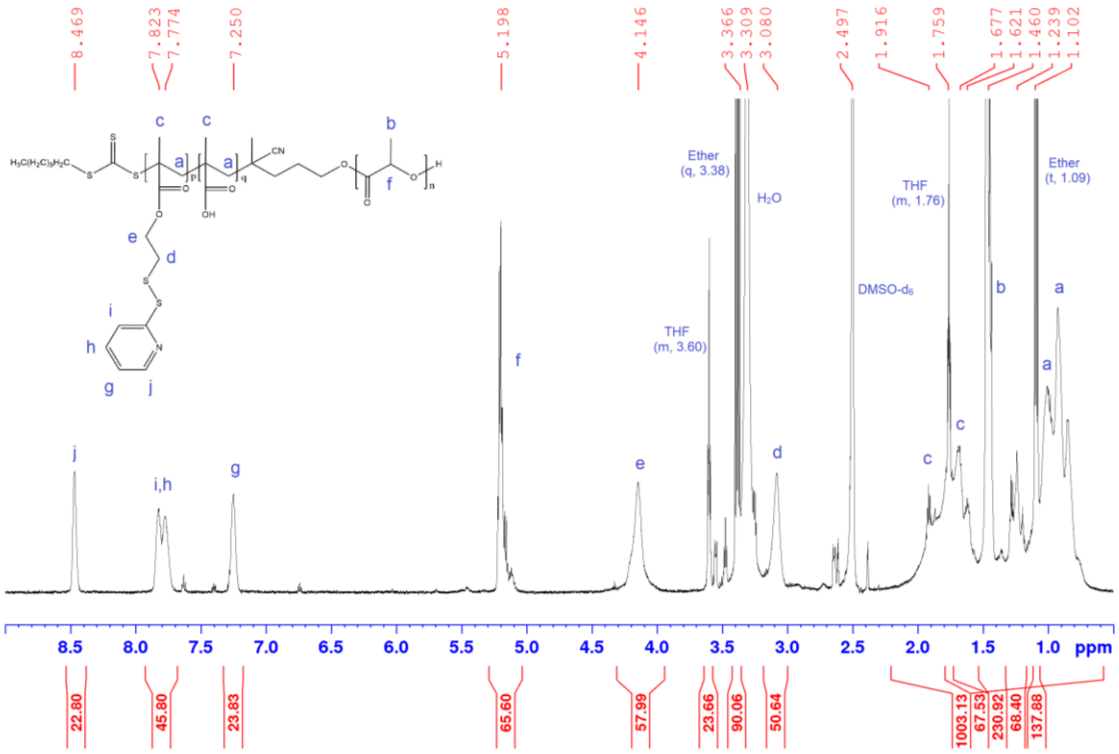

Figure 12. ^{1}H NMR spectrum of the LMS-20 polymer in DMSO-d_6. Elimination of acrylate peaks from δ [ppm] = 6.0 – 5.5 and introduction of methyl and ethyl peaks from polymer backbone at δ [ppm] = 2.0 – 0.5 indicate successful polymer synthesis. δ [ppm] = 8.5 – 7.0 (aromatic of PDSMA), 5.2 (C***H*** of lactide), 4.1 and 3.1 (ethyl of PDSMA), 2.0 – 0.5 (methyl and ethyl peaks of MAA), 2.0 – 0.5 (ethyl peaks associated with 3-AAPBA), 1.45 (methyl of lactide).

The chemical composition of the polymers was determined through proton integration of the ^{1}H NMR spectra. Commercially available PLA-CDP was analyzed by GPC and found to have a number average molecular weight (M_n) of 5115 g/mol, weight average molecular weight (M_w) of 5597 g/mol, and a PDI of 1.09. With the MW of the lactic acid repeat unit being 72.06 Da, and the non-repeat unit portion amounting to a MW of 388.4 Da, using the M_n from GPC, there are 65.6 repeat units per polymer chain. By integrating the NMR spectra for the

individual proton of PLA at δ = 5.2 to 65.6, it was possible to calculate and normalize the final monomer molar ratio and subsequently the molecular weight of the polymer. The results for both polymers are shown in Table 1.

Table 1. Polymerization data for LMP-20 and LMS-20 obtained from analysis of ^{1}H NMR chemical shift.

Polymer	Molecular Weight (g/mol)	Molar Feed Ratio (LA:MAA:3-AAPBA or PDSMA)	Final Molar Ratio (LA:MAA:3-AAPBA or PDSMA)	Ratio of MAA:3-AAPBA or PDSMA
LMP-20	19,932	50:40:10	32.3:53.7:14.0	3.8:1
LMS-20	20,556	50:40:10	33.6:54.5:11.9	4.6:1

The results in Table 1 show similar chemical composition and molecular weight between the two polymers. The final molecular weight of the polymers is ~ 20 kDa, which is an acceptable polymer MW for renal clearance (MWCO ~ 70 kDa) [98], an important property to ensure elimination of the material from the body. Properties of the LMP-20 polymer also agree with previous attempts at synthesis by the Sheardown Lab. The results show a higher amount of 3-AAPBA in LMP-20 compared to the amount of PDSMA in LMS-20, a difference amounting to a 23% increase in the number of 3-AAPBA groups (28 repeat units from ^{1}H NMR) compared to PDSMA groups (23 repeat units from ^{1}H NMR) per polymer. This result must be considered when analyzing results from mucoadhesive studies as these are the major mucoadhesive components of the polymers.

Due to issues encountered in the solubility of both polymers as a result of their amphiphilic nature, ^{1}H NMR was used to estimate the MW of each polymer. The

limitations on accuracy of MW determination from ^{1}H NMR suggest that future work should investigate a more robust method such as GPC to determine both the MW and the PDI of these polymers.

4.2.2. Post-Polymerization Modifications

Modifications to the LMS-20 polymer were required as the 2-pyridinethione leaving group can be cytotoxic [85]. Based on the literature suggesting that small, less reactive thiol molecules such as NAC can provide enhanced mucoadhesion in comparison to more reactive thiol ligands such as pyridine groups, the choice was made to modify LMS-20 with NAC, Cys, and GSH [90]. NAC was chosen as a model small molecule for modification as it has previously been reported to act as a mucoadhesive agent in a similar application in a preactivated thiomer [90], and is commercially available as a 5% w/v ophthalmic solution (Ilube® by Rayner) to treat DED. Modifications were made through a thiol/disulfide exchange reaction and results for the modification with NAC can be seen in the ^{1}H NMR spectrum comparison shown in Figure 13. The successful incorporation of NAC into the polymer resulted in elimination of PDS peaks between δ ~ 7.0 – 8.5 and the introduction of novel NAC peaks at δ ~ 8.3, 4.5, 3.2 and 1.9. Successful modifications were also performed with Cys and GSH, with the spectrums shown in Appendix B. However, difficulties with the nanoprecipitation method resulted in the discontinuation of the Cys and GSH modified polymers . Future work should investigate the solubility of LMC-20 and LMG-20 in different solvents to allow for

the use of nanoprecipitation to form micelles. In addition, the cytotoxicity of these novel formulations with corneal epithelial cells should be studied.

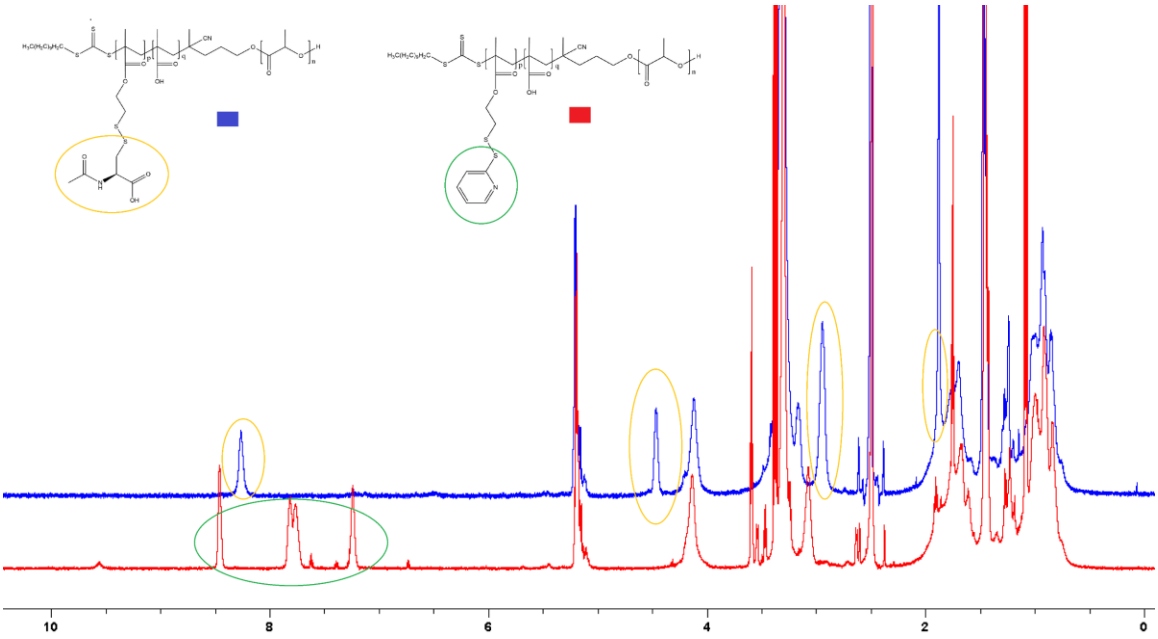

Figure 13. ^{1}H NMR spectra comparison between LMS-20 (red) and LMA-20 (blue). Yellow circles represent the new peaks attributable to the successful modification with NAC; green circles represent the peaks of the PDS group that can be seen to have disappeared following successful modification.

4.3. Nano-micelle Characterization

4.3.1. Particle Size & Morphology

The effective diameter and PDI of the micelles were determined by DLS (Table 2). A comparison between the LMP-20 and LMA-20 micelles reveals a significant difference (Tukey; $p < .001$) in their sizes. A significant increase in micelle size after Cyc-A loading was observed (Tukey; $p < .01$). Similar results for increased size after drug loading have been shown in the literature with loading of

dexamethasone into micelles [81], as well as previous results with Cyc-A loaded LMP-20 micelles (unpublished data). The PDI values for nanoparticles vary widely from fairly monodisperse distributions (< 0.05) to large distributions (> 0.7) [99]. The PDI of the LMA-20 and LMP-20 micelles is around 0.3, representing a wider distribution. These results are comparable to those obtained from other polymeric micelle formulations [39, 100, 101].

Table 2. LMP-20 and LMA-20 micelle size from DLS measurements. PDI values represent the mean (n=3). Effective diameter values represent the mean ± standard deviation (SD) (n=3).

	Empty Micelles		Cyc-A loaded Micelles	
Polymer	Effective Diameter (nm ± SD)	PDI	Effective Diameter (nm ± SD)	PDI
LMP-20	72 ± 3	0.30	-	-
LMA-20	64 ± 5	0.28	71 ± 5	0.32

The morphology of the micelles was determined by TEM (Figure 14). Spherical morphology was obtained and can be seen for both LMP-20 and LMA-20 micelles, with approximate size from the TEM images agreeing with the DLS results.

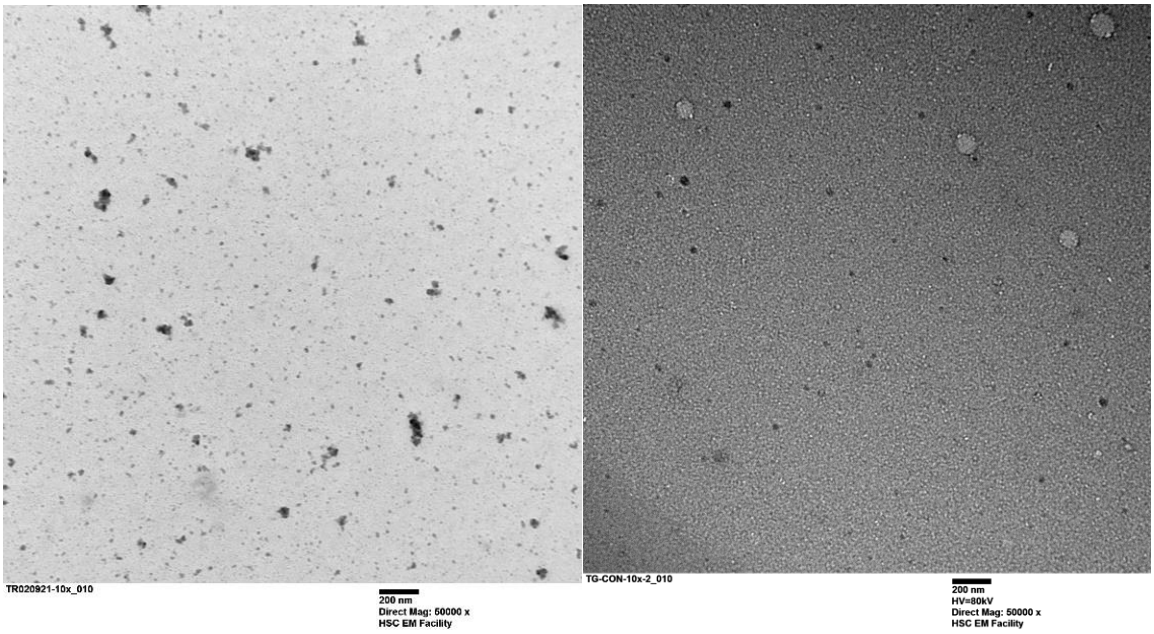

Figure 14. Transmission Electron Micrograph of the LMA-20 (left panel) and LMP-20 (right panel) micelles with distinct spherical morphology.

4.3.2. Critical Micelle Concentration

The CMC is an important parameter of a micellar drug delivery system as it provides insight into the system's stability. A CMC lower than the concentration of intended application is desirable as this ensures that the micelle will stay intact and not disassemble upon application. As LMP-20 has been previously shown to have a CMC below the concentration of intended application [39], only LMA-20 was investigated herein.

To measure the CMC, the pyrene fluorescence method was used in which different concentrations of LMA-20 micelle solution were incubated with a fixed concentration of pyrene. As the concentration of LMA-20 increases, the pyrene will preferentially partition into the hydrophobic core of the micelles and the ratio of the

intensity of the emitted light at λ = 373 nm and 383 nm will rapidly change (I_{373}/I_{383}) [102]. This result can be seen in Figure 15 where the CMC is determined as the intersection of the best fit line to the variable region with the nearly horizontal region at high polymer concentration [95]. A CMC of 217 mg/L was obtained for the LMA-20 polymer. For all practical applications of this formulation, such a low value for the CMC is considered acceptable. This is a highly conservative estimate as some in literature use the inflection point of the highly variable region, or the intersection of the highly variable region with the nearly horizontal region at low polymer concentration as the CMC, which would result in much lower values of the CMC [102, 103].

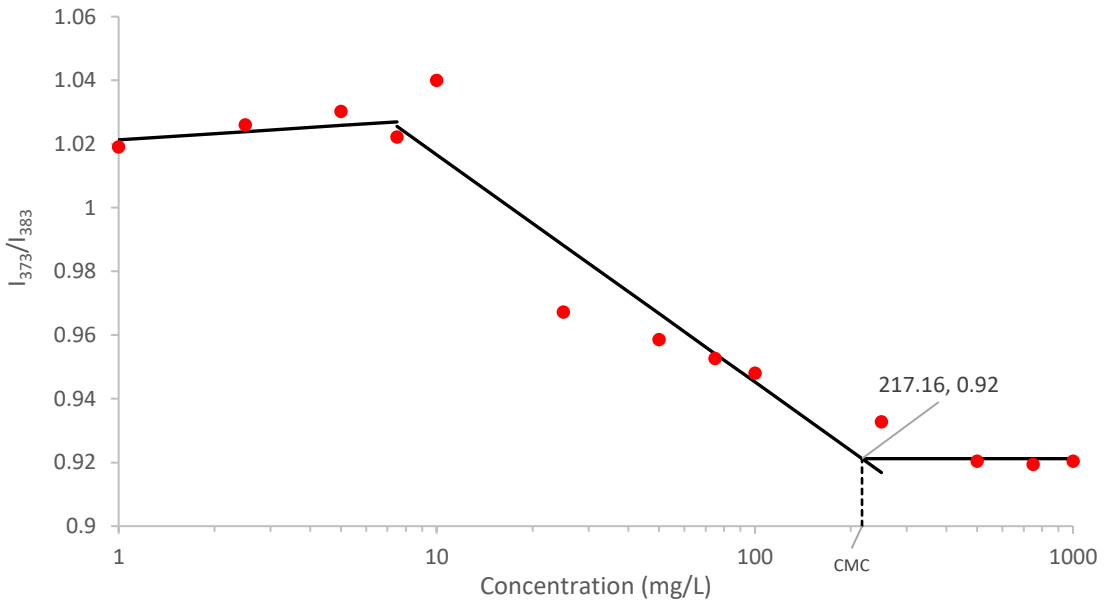

Figure 15. CMC as determined by the pyrene fluorescence intensity ratio at 373 nm and 383 nm, with excitation of 340 nm, measured at different concentrations of LMA-20 polymer in PBS (0.1M, pH 7.4). Concentration is plotted on a logarithmic scale. Each value represents the result from a single measurement (n=1).

4.3.3. Mucoadhesion (Zeta potential)

To determine whether the micelles were mucoadhesive, zeta potential studies were performed (Figure 16). Control samples of mucin, LMP-20 micelles, and LMA-20 micelles were run along with micelle/mucin mixtures. Control samples had a negative zeta potential. The negative charge of the mucin can be attributed to sialic acid and sulfate residues, while that of the micelles can be attributed to carboxylic acid groups in the hydrophilic shell of the micelles.

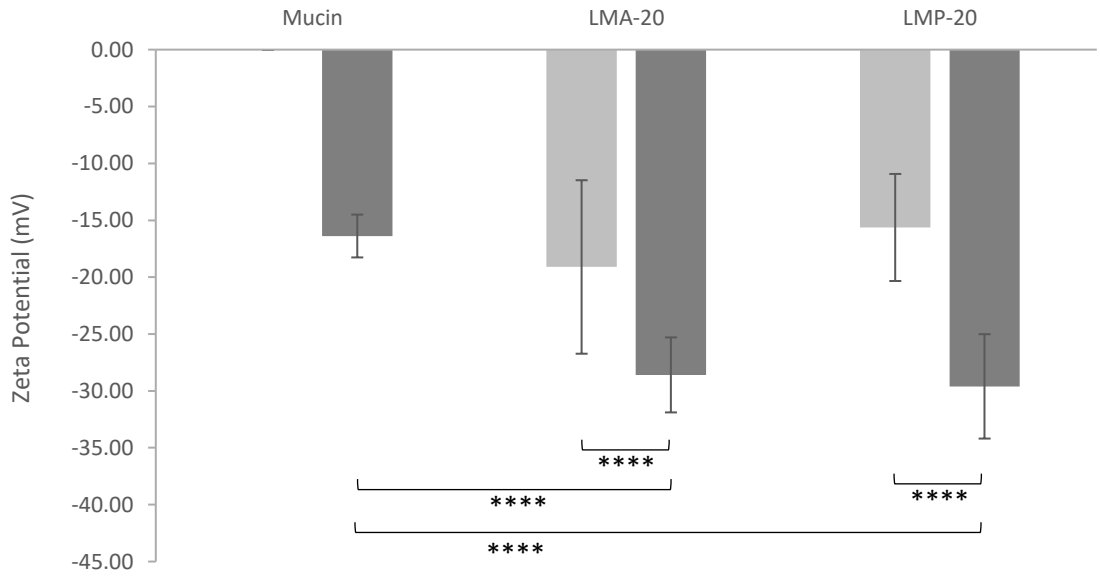

Figure 16. Zeta potential values for a mucin solution, LMA-20 sample, and LMP-20 sample, with (dark grey) and without (light grey) mucin. Each value represents the mean ± SD of 18 measurements (n = 3 samples). Welch's test; $p < .001$ (****). All samples prepared in 10 mM sodium phosphate salt.

The assumption is that a micelle/mucin mixture whose zeta potential is the same as either of the controls or that lies at an average value between the two controls, is not mucoadhesive. This is because it is not possible to determine

whether the change in zeta-potential was simply due to the addition of micelles to the mucin, creating an average value of the zeta potential between the two species in solution. It is then assumed that a significantly lower observed zeta potential between the micelle/mucin mixtures and their respective controls is due to mucin-particle interactions and not simply due to the mixture of the two [104]. As was observed in Figure 16, a highly significant decrease in the zeta potential was seen upon mixing the LMP-20 and LMA-20 micelles with mucin, with respect to their controls and the mucin control (Welch; $p < .001$). This interaction between mucin and NPs is typically attributed in the literature to the adsorption of mucin to the particle surface, coating the particle and resulting in a change in the surface charge of the particles [105]. Therefore, both LMP-20 and LMA-20 are predicted to be mucoadhesive, but further testing is required to validate mucoadhesion based on the limitations of the results of a single technique.

4.3.4. Mucoadhesion (Rheology)

To complement the zeta-potential study, a rheological investigation was performed to investigate mucoadhesive potential of the LMA-20 and LMP-20 micelles by oscillatory rheology. A theoretical value of the complex viscosity for the micelle/mucin mixture can be obtained by summing the complex viscosity of the micelle and mucin controls and comparing this to the experimental value obtained for the mixture. If the calculation for the rheological synergism results in a positive value that is significantly different from zero, then it is predicted that an interaction occurred between mucin and the micelle [106].

An oscillatory strain sweep was performed on all sample types to determine a strain in the linear viscoelastic region among all samples. To this end, a strain of 1% was chosen for the subsequent oscillatory frequency sweeps. The results were used to calculate the rheological synergism, which is reported in Figure 17 at an angular frequency of 10 s^{-1}. The rheological synergism in this study had a highly significantly difference from zero (Tukey; $p < .001$) and was negative for both LMA-20 and LMP-20 mixtures. This result is not unexpected as many have reported similar results for NP formulations, as well as some polymer formulations [67, 106-108]. As was reported by Hägerström and Edsman, it is possible that negative values of rheological synergism can result from an interaction between mucin and polymer, resulting in weaker, rather than stronger, properties of the mixture in comparison to the controls [109]. Eshel-Green and Bianco-Peled found similar negative synergism with their acrylated poloxamer micelles [107]. Their explanation for the phenomenon is that commercial mucin contains large aggregates which the micelles may be small enough to penetrate. Once the micelles penetrate these large aggregates, they separate the mucin glycoprotein chains from one another and adsorb individual mucin strands to their surface, resulting in degradation of the mucin aggregates, and under shear, reduction in viscosity [107]. However, further investigations into these mechanisms are required to state similar conclusions of the results presented herein. Therefore, these rheological studies provide inconclusive evidence of mucoadhesion for either micelle formulation. Based on the limitations of this technique [109], future

studies either *ex vivo* or *in vivo* would be beneficial in comparing the two formulations.

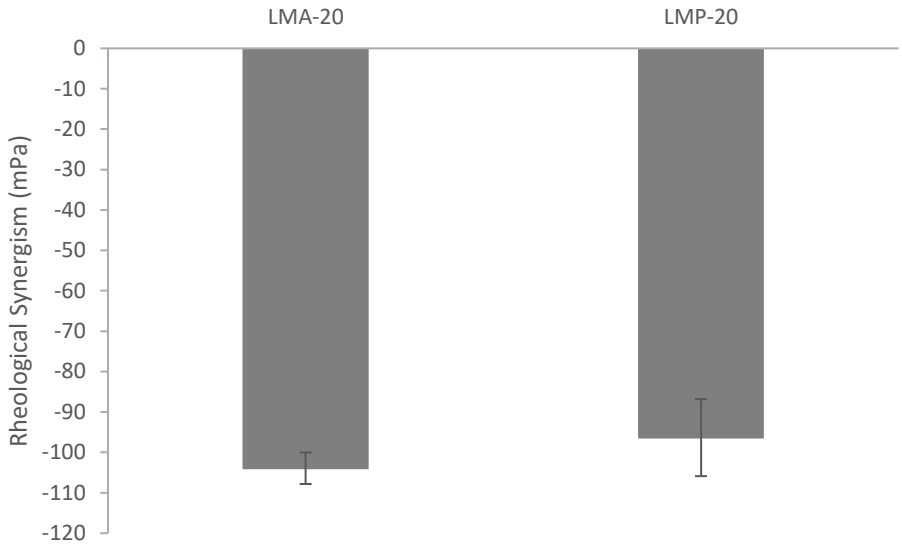

Figure 17. Rheological synergism as calculated from storage modulus for LMA-20 and LMP-20 experiments at an angular frequency of 10 s^{-1}. Values represent the mean ± SD (n=3). No statistical difference observed between the two micelle formulations (Tukey; $p > .05$).

4.4. Drug Release

Several relevant ocular therapeutics have been encapsulated effectively with the LMP-20 formulation in past work. However, the PBA group is thought to hinder the encapsulation of certain compounds. Therefore, in addition to providing a different method of binding to the mucin, altering the binding moiety may allow for the encapsulation of compounds that were unsuccessful with the LMP-20 formulation.

Cyc-A is an immunosuppressant drug employed in the therapeutic treatment of DED, commonly treated with the topical instillation of eye drops [110]. Many in academia and industry have been developing mucoadhesive formulations to compete with the market staple Restasis® (0.05 % w/w Cyc-A ophthalmic emulsion) [39, 43, 56]. The Sheardown Lab has previously shown the ability to encapsulate Cyc-A using the LMP-20 formulation [39]. Therefore, Cyc-A represented an appropriate starting point.

Prior to performing a drug release, the EE and DL content of the LMA-20 micelle formulation was investigated, and results are reported in Table 3. The LMA-20 micelles had an EE of 90.6 ± 7.4%, forming a 0.16% (w/w) Cyc-A formulation. Prosperi-Porta *et al*. reportedly obtained a DL of 15% (w/w) for the LMP-20 micelles loaded with Cyc-A [39]. Unpublished results have shown similar DL of 13-15% (w/w) for LMP-20 batches of similar composition to those produced herein. In comparison to the market leader for DED treatment Restasis®, the LMA-20 micelles entrap ~ 3x the amount of Cyc-A.

Table 3. Drug EE and DL of LMA-20 polymeric micelles with Cyc-A. All numbers represent the mean ± SD (n = 3).

	Cyc-A Feed (mg/mL; ± SD)	Entrapped Cyc-A (mg/mL; ± SD)	EE (%; ± SD)	DL (% w/w; ± SD)
LMA-20	1.76 ± 0.28	1.61 ± 0.37	90.6 ± 7.4	13.8 ± 2.8

Release of Cyc-A from the LMA-20 micelles was studied *in vitro* to understand the potential use of the formulation for delivery of ocular therapeutics. Results in Figure 18 indicate a sustained release up to 3 days, with the concentration in

solution levelling off after 3 days. The LMA-20 micelles were able to release 57.5% (231 µg) of the entrapped drug after 10 days. It is possible that further release from the LMA-20 micelles could be expected after 10 days, however sampling was only done up to 10 days as the micelles are expected to be cleared from the ocular surface by this time due to the rapid tear/mucin turnover rate.

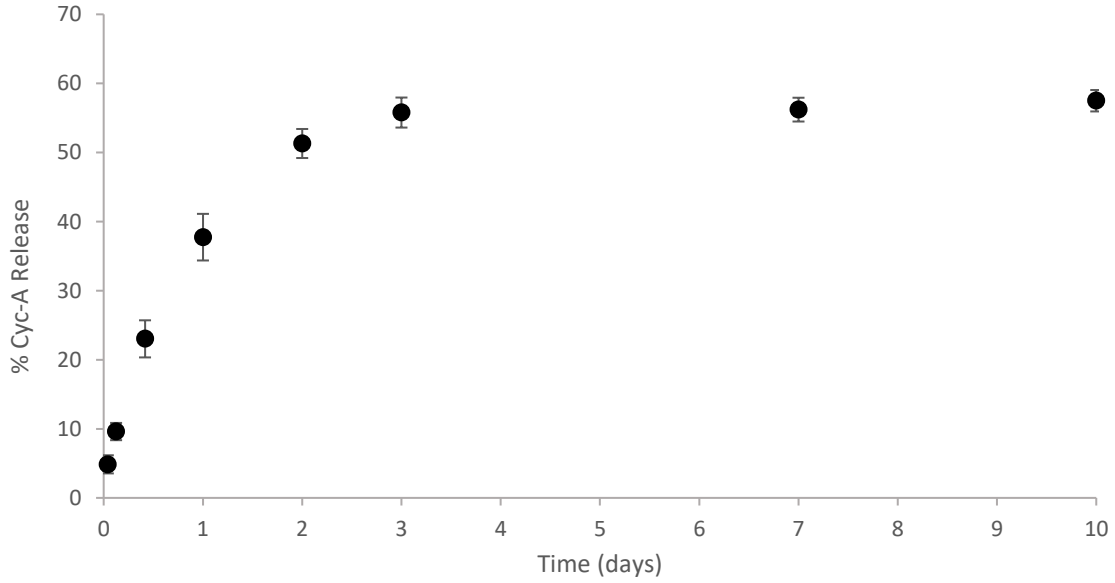

Figure 18. Cumulative release profile of Cyc-A from LMA-20 micelle formulation (0.16% Cyc-A formulation) in 0.1M PBS (pH 7.4). Each value represents the mean ± SD (n=3).

5. CONCLUSIONS

In conclusion, preactivated thiomer-based micelles which have the potential to improve mucoadhesion and provide sustained release of relevant ocular therapeutics were successfully synthesized. A preactivated thiol monomer was synthesized (PDSMA) as confirmed by ^{1}H NMR. Incorporation of this monomer in the synthesis of the amphiphilic block copolymer LMS-20 was confirmed by ^{1}H NMR. A Sheardown Lab designed amphiphilic block copolymer containing 3-AAPBA (LMP-20) was synthesized to investigate mucoadhesion imparted by the PBA and preactivated thiomer of LMS-20. Modifications of LMS-20 with small thiol molecules GSH, Cys, and NAC (LMG-20, LMC-20, and LMA-20 respectively) were made to reduce potential toxicity and successful synthesis was confirmed with ^{1}H NMR by the loss of aromatic peaks associated with 2-pyridinethione and incorporation of peaks associated with the respective thiol compounds. LMA-20 was chosen to move forward with for the purposes of this work as it contained the most relevant thiol modification for ocular applications and was capable of nanoprecipitation to form aqueous micelles with known methods. Aqueous micelles of LMA-20 and LMP-20 were formed with effective diameters of 64 ± 5 nm and 72 ± 3 nm, respectively, as confirmed by DLS. The morphology of the micelles was spherical as confirmed by TEM. Further confirmation of micelle formation was obtained through a measure of the fluorescence intensity of pyrene in solutions containing different concentrations of the LMA-20 polymer, resulting in a value for the critical micelle concentration of 217 mg/L. Both LMA-20 and LMP-

20 were suggested to be mucoadhesive based on zeta-potential studies showing a statistically significant decrease in the zeta-potential of the micelles after incubation with mucin. Mucoadhesion of both micelle formulations was further investigated with oscillatory rheology studies, which demonstrated a significant negative rheological synergism for both LMA-20 and LMP-20. These results provide inconclusive evidence for mucoadhesion of LMA-20 or LMP-20. Limitations of both methods for testing mucoadhesion suggest further investigation is required using *ex vivo* or *in vivo* studies. LMA-20 micelles were able to entrap 3x the amount of Cyc-A as the market leader Restasis® and release of Cyc-A from the micelles showed sustained release up to 3 days. These results suggest the potential future development of these materials as a mucoadhesive drug delivery system for the treatment of diseases of the anterior segment.

Future work should begin by investigating the cytotoxicity of the LMA-20 formulation. Investigations of the mucoadhesion of LMA-20 in comparison to LMP-20 micelles *ex vivo* or *in vivo* should then be performed by testing the residence time on the ocular surface and in anterior ocular tissues. Optimization of the synthesis of the PDSMA monomer and subsequent LMS-20 polymer to improve yield would be beneficial. Improvements could be made in the nanoprecipitation process to allow for a wider range of applicable small thiol modifications to LMS-20. Drug loading and encapsulation efficiency of Cyc-A in the LMA-20 micelles could be improved by performing a design of experiments. In addition, encapsulation of other relevant ocular therapeutics to produce a drug library would

provide insight into the applicability of these formulations for the treatment of a breadth of ocular diseases.

6. REFERENCES

[1] R. D. Bachu, P. Chowdhury, Z. H. F. Al-Saedi, P. K. Karla, and S. H. S. Boddu, "Ocular Drug Delivery Barriers-Role of Nanocarriers in the Treatment of Anterior Segment Ocular Diseases," *Pharmaceutics,* vol. 10, no. 1, Feb 27 2018, doi: 10.3390/pharmaceutics10010028.

[2] N. M. Davies, "Biopharmaceutical Considerations In Topical Ocular Drug Delivery," *Clinical and Experimental Pharmacology and Physiology,* vol. 27, no. 7, pp. 558-562, 2000, doi: 10.1046/j.1440-1681.2000.03288.x.

[3] K. Hosoya, V. H. Lee, and K. J. Kim, "Roles of the conjunctiva in ocular drug delivery: a review of conjunctival transport mechanisms and their regulation," *Eur J Pharm Biopharm,* vol. 60, no. 2, pp. 227-40, Jul 2005, doi: 10.1016/j.ejpb.2004.12.007.

[4] R. Gaudana, H. K. Ananthula, A. Parenky, and A. K. Mitra, "Ocular drug delivery," *AAPS J,* vol. 12, no. 3, pp. 348-60, Sep 2010, doi: 10.1208/s12248-010-9183-3.

[5] D. R. Janagam, L. Wu, and T. L. Lowe, "Nanoparticles for drug delivery to the anterior segment of the eye," *Adv Drug Deliv Rev,* vol. 122, pp. 31-64, Dec 1 2017, doi: 10.1016/j.addr.2017.04.001.

[6] C. H. Tsai, P. Y. Wang, I. C. Lin, H. Huang, G. S. Liu, and C. L. Tseng, "Ocular Drug Delivery: Role of Degradable Polymeric Nanocarriers for Ophthalmic Application," *Int J Mol Sci,* vol. 19, no. 9, Sep 19 2018, doi: 10.3390/ijms19092830.

[7] V. Gote, S. Sikder, J. Sicotte, and D. Pal, "Ocular Drug Delivery: Present Innovations and Future Challenges," *J Pharmacol Exp Ther,* vol. 370, no. 3, pp. 602-624, Sep 2019, doi: 10.1124/jpet.119.256933.

[8] H. Chen *et al.*, "Recent Developments in Ophthalmic Drug Delivery Systems for Therapy of Both Anterior and Posterior Segment Diseases," *Colloid and Interface Science Communications,* vol. 24, pp. 54-61, 2018, doi: 10.1016/j.colcom.2018.03.008.

[9] F. A. Maulvi, T. G. Soni, and D. O. Shah, "A review on therapeutic contact lenses for ocular drug delivery," *Drug Deliv,* vol. 23, no. 8, pp. 3017-3026, Oct 2016, doi: 10.3109/10717544.2016.1138342.

[10] P. Schattling, E. Taipaleenmaki, Y. Zhang, and B. Stadler, "A Polymer Chemistry Point of View on Mucoadhesion and Mucopenetration," *Macromol Biosci,* vol. 17, no. 9, Sep 2017, doi: 10.1002/mabi.201700060.

[11] T. F. Freddo, *Anatomy of the Eye and Orbit: The Clinical Essentials*. Philadelphia: Wolters Kluwer Heath, 2018.

[12] H. Lorentz and H. Sheardown, "Ocular Delivery of Biopharmaceuticals," in *Mucosal Delivery of Biopharmaceuticals: Biology, Challenges & Strategies*, J. das Neves and B. Sarmento Eds. New York: Springer Science+Business Media, 2014, ch. 9, pp. 221-259.

[13] B. Yanez-Soto *et al.*, "Interfacial phenomena and the ocular surface," *Ocul Surf,* vol. 12, no. 3, pp. 178-201, Jul 2014, doi: 10.1016/j.jtos.2014.01.004.
[14] F. Taherali, F. Varum, and A. W. Basit, "A slippery slope: On the origin, role and physiology of mucus," *Adv Drug Deliv Rev,* vol. 124, pp. 16-33, Jan 15 2018, doi: 10.1016/j.addr.2017.10.014.
[15] A. P. Corfield, "Mucins: a biologically relevant glycan barrier in mucosal protection," *Biochim Biophys Acta,* vol. 1850, no. 1, pp. 236-52, Jan 2015, doi: 10.1016/j.bbagen.2014.05.003.
[16] M. Ruponen and A. Urtti, "Undefined role of mucus as a barrier in ocular drug delivery," *Eur J Pharm Biopharm,* vol. 96, pp. 442-6, Oct 2015, doi: 10.1016/j.ejpb.2015.02.032.
[17] V. V. Khutoryanskiy, "Advances in Mucoadhesion and Mucoadhesive Polymers," *Macromolecular Bioscience,* vol. 11, no. 6, pp. 748-764, 2011, doi: 10.1002/mabi.201000388.
[18] J. D. Smart, "The basics and underlying mechanisms of mucoadhesion," *Advanced Drug Delivery Reviews,* vol. 57, no. 11, pp. 1556-1568, 2005/11/03/ 2005, doi: 10.1016/j.addr.2005.07.001.
[19] L. R. Schopf *et al.*, "Topical Ocular Drug Delivery to the Back of the Eye by Mucus-Penetrating Particles," *Transl Vis Sci Technol,* vol. 4, no. 3, p. 11, Jun 2015, doi: 10.1167/tvst.4.3.11.
[20] S. L. Gerber, L. B. Cantor, and D. C. Brater, "Systemic drug interactions with topical glaucoma medications," *Survey of Ophthalmology,* vol. 35, no. 3, pp. 205-218, 1990/11/01/ 1990, doi: 10.1016/0039-6257(90)90090-I.
[21] A. Urtti, "Challenges and obstacles of ocular pharmacokinetics and drug delivery," *Adv Drug Deliv Rev,* vol. 58, no. 11, pp. 1131-5, Nov 15 2006, doi: 10.1016/j.addr.2006.07.027.
[22] X.-j. Yi, Y. Wang, and F.-S. X. Yu, "Corneal Epithelial Tight Junctions and Their Response to Lipopolysaccharide Challenge," *Investigative Ophthalmology & Visual Science,* vol. 41, no. 13, pp. 4093-4100, 2000.
[23] D. M. Maurice, "The structure and transparency of the cornea," *The Journal of Physiology,* vol. 136, no. 2, pp. 263-286, 1957, doi: 10.1113/jphysiol.1957.sp005758.
[24] P. G. Watson and R. D. Young, "Scleral structure, organisation and disease. A review," *Experimental Eye Research,* vol. 78, no. 3, pp. 609-623, 2004/03/01/ 2004, doi: 10.1016/S0014-4835(03)00212-4.
[25] F. C. Carvalho, M. L. Bruschi, R. C. Evangelista, and M. P. D. Gremião, "Mucoadhesive drug delivery systems," *Brazilian Journal of Pharmaceutical Sciences,* vol. 46, pp. 1-17, 2010, doi: 10.1590/S1984-82502010000100002.
[26] Y. Huang, W. Leobandung, A. Foss, and N. A. Peppas, "Molecular aspects of muco- and bioadhesion: Tethered structures and site-specific surfaces," *Journal of Controlled Release,* vol. 65, no. 1, pp. 63-71, 2000/03/01/ 2000, doi: 10.160/S0168-3659(99)00233-3.

[27] N. A. Peppas and J. J. Sahlin, "Hydrogels as mucoadhesive and bioadhesive materials: a review," *Biomaterials,* vol. 17, no. 16, pp. 1553-1561, 1996/01/01/ 1996, doi: https://doi.org/10.1016/0142-9612(95)00307-X.

[28] P. Sriamornsak, N. Wattanakorn, J. Nunthanid, and S. Puttipipatkhachorn, "Mucoadhesion of pectin as evidence by wettability and chain interpenetration," *Carbohydrate Polymers,* vol. 74, no. 3, pp. 458-467, 2008/11/04/ 2008, doi: https://doi.org/10.1016/j.carbpol.2008.03.022.

[29] N. A. Peppas and Y. Huang, "Nanoscale technology of mucoadhesive interactions," *Advanced Drug Delivery Reviews,* vol. 56, no. 11, pp. 1675-1687, 2004/09/22/ 2004, doi: https://doi.org/10.1016/j.addr.2004.03.001.

[30] C.-M. Lehr, J. A. Bouwstra, H. E. Boddé, and H. E. Junginger, "A Surface Energy Analysis of Mucoadhesion: Contact Angle Measurements on Polycarbophil and Pig Intestinal Mucosa in Physiologically Relevant Fluids," *Pharmaceutical Research,* vol. 9, no. 1, pp. 70-75, 1992/01/01 1992, doi: 10.1023/A:1018931811189.

[31] R. Gurny, J.-M. Meyer, and N. A. Peppas, "Bioadhesive intraoral release systems: design, testing and analysis," *Biomaterials,* vol. 5, no. 6, pp. 336-340, 1984/11/01/ 1984, doi: https://doi.org/10.1016/0142-9612(84)90031-0.

[32] F. Laffleur, "Mucoadhesive polymers for buccal drug delivery," *Drug Development and Industrial Pharmacy,* vol. 40, no. 5, pp. 591-598, 2014/05/01 2014, doi: 10.3109/03639045.2014.892959.

[33] R. V. Pai and P. R. Vavia, "Chitosan oligosaccharide enhances binding of nanostructured lipid carriers to ocular mucins: Effect on ocular disposition," *Int J Pharm,* vol. 577, p. 119095, Mar 15 2020, doi: 10.1016/j.ijpharm.2020.119095.

[34] I. Bravo-Osuna, C. Vauthier, A. Farabollini, G. F. Palmieri, and G. Ponchel, "Mucoadhesion mechanism of chitosan and thiolated chitosan-poly(isobutyl cyanoacrylate) core-shell nanoparticles," *Biomaterials,* vol. 28, no. 13, pp. 2233-2243, 2007/05/01/ 2007, doi: https://doi.org/10.1016/j.biomaterials.2007.01.005.

[35] Y. Y. Wang, S. K. Lai, C. So, C. Schneider, R. Cone, and J. Hanes, "Mucoadhesive nanoparticles may disrupt the protective human mucus barrier by altering its microstructure," *PLoS One,* vol. 6, no. 6, p. e21547, 2011, doi: 10.1371/journal.pone.0021547.

[36] A. Bernkop-Schnürch and S. Steininger, "Synthesis and characterisation of mucoadhesive thiolated polymers," *International Journal of Pharmaceutics,* vol. 194, no. 2, pp. 239-247, 2000/01/25/ 2000, doi: https://doi.org/10.1016/S0378-5173(99)00387-7.

[37] C. Menzel, S. Bonengel, I. Pereira de Sousa, F. Laffleur, F. Prufert, and A. Bernkop-Schnurch, "Preactivated thiolated nanoparticles: A novel mucoadhesive dosage form," *Int J Pharm,* vol. 497, no. 1-2, pp. 123-8, Jan 30 2016, doi: 10.1016/j.ijpharm.2015.11.037.

[38] C. Li, Z. Liu, X. Yan, W. Lu, and Y. Liu, "Mucin-controlled drug release from mucoadhesive phenylboronic acid-rich nanoparticles," *International Journal of Pharmaceutics,* vol. 479, no. 1, pp. 261-264, 2015/02/01/ 2015, doi: https://doi.org/10.1016/j.ijpharm.2014.12.011.

[39] G. Prosperi-Porta, S. Kedzior, B. Muirhead, and H. Sheardown, "Phenylboronic-Acid-Based Polymeric Micelles for Mucoadhesive Anterior Segment Ocular Drug Delivery," *Biomacromolecules,* vol. 17, no. 4, pp. 1449-57, Apr 11 2016, doi: 10.1021/acs.biomac.6b00054.

[40] S. Köllner, S. Dünnhaupt, C. Waldner, S. Hauptstein, I. Pereira de Sousa, and A. Bernkop-Schnürch, "Mucus permeating thiomer nanoparticles," *European Journal of Pharmaceutics and Biopharmaceutics,* vol. 97, pp. 265-272, 2015/11/01/ 2015, doi: https://doi.org/10.1016/j.ejpb.2015.01.004.

[41] A. Bernkop-Schnürch, "Mucoadhesive systems in oral drug delivery," *Drug Discovery Today: Technologies,* vol. 2, no. 1, pp. 83-87, 2005/03/01/ 2005, doi: https://doi.org/10.1016/j.ddtec.2005.05.001.

[42] H. Takeuchi, H. Yamamoto, and Y. Kawashima, "Mucoadhesive nanoparticulate systems for peptide drug delivery," *Advanced Drug Delivery Reviews,* vol. 47, no. 1, pp. 39-54, 2001/03/23/ 2001, doi: https://doi.org/10.1016/S0169-409X(00)00120-4.

[43] S. Liu *et al.*, "Prolonged Ocular Retention of Mucoadhesive Nanoparticle Eye Drop Formulation Enables Treatment of Eye Diseases Using Significantly Reduced Dosage," *Mol Pharm,* vol. 13, no. 9, pp. 2897-905, Sep 6 2016, doi: 10.1021/acs.molpharmaceut.6b00445.

[44] E. Iyamu and O. Enobakhare, "pH and Osmolality of Pre-Corneal Tear Film and Commercially Available Artificial Tears," *EC Ophthalmology,* vol. 10, no. 11, pp. 17-25, 2019.

[45] N. Nikonenko, I. Bushnak, and J. Keddie, "Spectroscopic Ellipsometry of Mucin Layers on an Amphiphilic Diblock Copolymer Surface," *Applied Spectroscopy,* vol. 63, no. 8, pp. 889-898, 2009, doi: https://doi.org/10.1366%2F000370209788964449.

[46] T. K. De, E. J. Bergey, S. J. Chung, D. J. Rodman, D. J. Bharali, and P. N. Prasad, "Polycarboxylic acid nanoparticles for ophthalmic drug delivery: an ex vivo evaluation with human cornea," *J Microencapsul,* vol. 21, no. 8, pp. 841-55, Dec 2004, doi: 10.1080/02652040400008515.

[47] H. A. Abd El-Rehim, A. E. Swilem, A. Klingner, S. A. Hegazy el, and A. A. Hamed, "Developing the potential ophthalmic applications of pilocarpine entrapped into polyvinylpyrrolidone-poly(acrylic acid) nanogel dispersions prepared by gamma radiation," *Biomacromolecules,* vol. 14, no. 3, pp. 688-98, Mar 11 2013, doi: 10.1021/bm301742m.

[48] A. Račić, B. Čalija, J. Milić, N. Milašinović, and D. Krajišnik, "Development of polysaccharide-based mucoadhesive ophthalmic lubricating vehicles: The effect of different polymers on physicochemical properties and functionality," *Journal of Drug Delivery Science and Technology,* vol. 49,

pp. 50-57, 2019/02/01/ 2019, doi: https://doi.org/10.1016/j.jddst.2018.10.034.

[49] R. Ilka, M. Mohseni, M. Kianirad, M. Naseripour, K. Ashtari, and B. Mehravi, "Nanogel-based natural polymers as smart carriers for the controlled delivery of Timolol Maleate through the cornea for glaucoma," *Int J Biol Macromol,* vol. 109, pp. 955-962, Apr 1 2018, doi: 10.1016/j.ijbiomac.2017.11.090.

[50] A. Graca, L. M. Goncalves, S. Raposo, H. M. Ribeiro, and J. Marto, "Useful In Vitro Techniques to Evaluate the Mucoadhesive Properties of Hyaluronic Acid-Based Ocular Delivery Systems," *Pharmaceutics,* vol. 10, no. 3, Aug 1 2018, doi: 10.3390/pharmaceutics10030110.

[51] W. Zeng *et al.*, "Hyaluronic acid-coated niosomes facilitate tacrolimus ocular delivery: Mucoadhesion, precorneal retention, aqueous humor pharmacokinetics, and transcorneal permeability," *Colloids Surf B Biointerfaces,* vol. 141, pp. 28-35, May 1 2016, doi: 10.1016/j.colsurfb.2016.01.014.

[52] B. Silva, J. Marto, B. S. Braz, E. Delgado, A. J. Almeida, and L. Goncalves, "New nanoparticles for topical ocular delivery of erythropoietin," *Int J Pharm,* vol. 576, p. 119020, Feb 25 2020, doi: 10.1016/j.ijpharm.2020.119020.

[53] M. A. Kalam, "The potential application of hyaluronic acid coated chitosan nanoparticles in ocular delivery of dexamethasone," *Int J Biol Macromol,* vol. 89, pp. 559-68, Aug 2016, doi: 10.1016/j.ijbiomac.2016.05.016.

[54] D. Liu, Y. Lian, Q. Fang, L. Liu, J. Zhang, and J. Li, "Hyaluronic-acid-modified lipid-polymer hybrid nanoparticles as an efficient ocular delivery platform for moxifloxacin hydrochloride," *Int J Biol Macromol,* vol. 116, pp. 1026-1036, Sep 2018, doi: 10.1016/j.ijbiomac.2018.05.113.

[55] H. Y. Huang *et al.*, "Gelatin-epigallocatechin gallate nanoparticles with hyaluronic acid decoration as eye drops can treat rabbit dry-eye syndrome effectively via inflammatory relief," *Int J Nanomedicine,* vol. 13, pp. 7251-7273, 2018, doi: 10.2147/IJN.S173198.

[56] E. Terreni *et al.*, "Assembling Surfactants-Mucoadhesive Polymer Nanomicelles (ASMP-Nano) for Ocular Delivery of Cyclosporine-A," *Pharmaceutics,* vol. 12, no. 3, Mar 11 2020, doi: 10.3390/pharmaceutics12030253.

[57] A. Mahor, S. K. Prajapati, A. Verma, R. Gupta, A. K. Iyer, and P. Kesharwani, "Moxifloxacin loaded gelatin nanoparticles for ocular delivery: Formulation and in-vitro, in-vivo evaluation," *J Colloid Interface Sci,* vol. 483, pp. 132-138, Dec 1 2016, doi: 10.1016/j.jcis.2016.08.018.

[58] M. J. Alonso and A. Sanchez, "The potential of chitosan in ocular drug delivery," *J Pharm Pharmacol,* vol. 55, no. 11, pp. 1451-63, Nov 2003, doi: 10.1211/0022357022476.

[59] V. Dodane, M. A. Khan, and J. R. Merwin, "Effect of chitosan on epithelial permeability and structure," *Int J Pharm,* vol. 182, pp. 21-32, 1999.

[60] M. Collado-Gonzalez, Y. Gonzalez Espinosa, and F. M. Goycoolea, "Interaction Between Chitosan and Mucin: Fundamentals and Applications," *Biomimetics (Basel),* vol. 4, no. 2, Apr 25 2019, doi: 10.3390/biomimetics4020032.

[61] S. B. da Silva, D. Ferreira, M. Pintado, and B. Sarmento, "Chitosan-based nanoparticles for rosmarinic acid ocular delivery—In vitro tests," *International Journal of Biological Macromolecules,* vol. 84, pp. 112-120, 2016/03/01/ 2016, doi: https://doi.org/10.1016/j.ijbiomac.2015.11.070.

[62] W. Chaiyasan, S. P. Srinivas, and W. Tiyaboonchai, "Crosslinked chitosan-dextran sulfate nanoparticle for improved topical ocular drug delivery," (in eng), *Mol Vis,* vol. 21, pp. 1224-1234, 2015. [Online]. Available: https://www.ncbi.nlm.nih.gov/pmc/articles/PMC4626781/.

[63] A. Yu *et al.*, "Mucoadhesive dexamethasone-glycol chitosan nanoparticles for ophthalmic drug delivery," *Int J Pharm,* vol. 575, p. 118943, Feb 15 2020, doi: 10.1016/j.ijpharm.2019.118943.

[64] A. M. Piras *et al.*, "A water-soluble, mucoadhesive quaternary ammonium chitosan-methyl-beta-cyclodextrin conjugate forming inclusion complexes with dexamethasone," *J Mater Sci Mater Med,* vol. 29, no. 4, p. 42, Mar 30 2018, doi: 10.1007/s10856-018-6048-2.

[65] S. Manchanda and P. K. Sahoo, "Fabrication and characterization of mucoadhesive topical nanoformulations of dorzolamide HCl for ocular hypertension," *Journal of Pharmaceutical Investigation,* vol. 48, no. 3, pp. 323-332, 2017, doi: 10.1007/s40005-017-0324-x.

[66] S. Taghe and S. Mirzaeei, "Preparation and characterization of novel, mucoadhesive ofloxacin nanoparticles for ocular drug delivery," *Brazilian Journal of Pharmaceutical Sciences,* vol. 55, 2019, doi: 10.1590/s2175-97902019000117105.

[67] M. M. Silva, R. Calado, J. Marto, A. Bettencourt, A. J. Almeida, and L. M. D. Goncalves, "Chitosan Nanoparticles as a Mucoadhesive Drug Delivery System for Ocular Administration," *Mar Drugs,* vol. 15, no. 12, Dec 1 2017, doi: 10.3390/md15120370.

[68] W. H. Abd-Elsalam and N. A. ElKasabgy, "Mucoadhesive olaminosomes: A novel prolonged release nanocarrier of agomelatine for the treatment of ocular hypertension," *Int J Pharm,* vol. 560, pp. 235-245, Apr 5 2019, doi: 10.1016/j.ijpharm.2019.01.070.

[69] H. R. Lin, S. P. Yu, C. J. Kuo, H. J. Kao, Y. L. Lo, and Y. J. Lin, "Pilocarpine-loaded chitosan-PAA nanosuspension for ophthalmic delivery," *J Biomater Sci Polym Ed,* vol. 18, no. 2, pp. 205-21, 2007, doi: 10.1163/156856207779116739.

[70] H. C. Wang *et al.*, "A bis-boronic acid modified electrode for the sensitive and selective determination of glucose concentrations," *Analyst,* vol. 138, no. 23, pp. 7146-51, Dec 7 2013, doi: 10.1039/c3an01234d.

[71] D. Hall, "Structure, Properties, and Preparation of Boronic Acid Derivatives. Overview of Their Reactions and Applications," in *Boronic*

Acids: Preparation and Applications in Organic Synthesis and Medicine. Germany: Wiley-VCH, 2005, ch. 1, pp. 1-19.

[72] T. Elshaarani *et al.*, "Synthesis of hydrogel-bearing phenylboronic acid moieties and their applications in glucose sensing and insulin delivery," *J Mater Chem B,* vol. 6, no. 23, pp. 3831-3854, Jun 21 2018, doi: 10.1039/c7tb03332j.

[73] H. C. Wang and A. R. Lee, "Recent developments in blood glucose sensors," *J Food Drug Anal,* vol. 23, no. 2, pp. 191-200, Jun 2015, doi: 10.1016/j.jfda.2014.12.001.

[74] S. Liu, L. Jones, and F. X. Gu, "Development of mucoadhesive drug delivery system using phenylboronic acid functionalized poly(D,L-lactide)-b-dextran nanoparticles," *Macromol Biosci,* vol. 12, no. 12, pp. 1622-6, Dec 2012, doi: 10.1002/mabi.201200216.

[75] G. Tan, J. Li, Y. Song, Y. Yu, D. Liu, and W. Pan, "Phenylboronic acid-tethered chondroitin sulfate-based mucoadhesive nanostructured lipid carriers for the treatment of dry eye syndrome," *Acta Biomater,* vol. 99, pp. 350-362, Nov 2019, doi: 10.1016/j.actbio.2019.08.035.

[76] A. Bernkop-Schnurch, C. E. Kast, and D. Guggi, "Permeation enhancing polymers in oral delivery of hydrophilic macromolecules: thiomer/GSH systems," *J Control Release,* vol. 93, no. 2, pp. 95-103, Dec 5 2003, doi: 10.1016/j.jconrel.2003.05.001.

[77] A. Bernkop-Schnürch and S. Steinenger, "Synthesis and Characterization of Mucoadhesive Thiolated Polymers," *Int J Pharm,* vol. 194, pp. 239-247, 1999.

[78] X. Zhu *et al.*, "Synthesis of thiolated chitosan and preparation nanoparticles with sodium alginate for ocular drug delivery," (in eng), *Mol Vis,* vol. 18, pp. 1973-1982, 2012. [Online]. Available: https://www.ncbi.nlm.nih.gov/pmc/articles/PMC3413446/.

[79] J. Li, D. Liu, G. Tan, Z. Zhao, X. Yang, and W. Pan, "A comparative study on the efficiency of chitosan-N-acetylcysteine, chitosan oligosaccharides or carboxymethyl chitosan surface modified nanostructured lipid carrier for ophthalmic delivery of curcumin," *Carbohydr Polym,* vol. 146, pp. 435-44, Aug 1 2016, doi: 10.1016/j.carbpol.2016.03.079.

[80] G. Horvát *et al.*, "Thiolated poly(aspartic acid) as potential in situ gelling, ocular mucoadhesive drug delivery system," *European Journal of Pharmaceutical Sciences,* vol. 67, pp. 1-11, 2015/01/25/ 2015, doi: https://doi.org/10.1016/j.ejps.2014.10.013.

[81] J. Yang, J. Yan, Z. Zhou, and B. G. Amsden, "Dithiol-PEG-PDLLA micelles: preparation and evaluation as potential topical ocular delivery vehicle," *Biomacromolecules,* vol. 15, no. 4, pp. 1346-54, Apr 14 2014, doi: 10.1021/bm4018879.

[82] A. Partenhauser and A. Bernkop-Schnurch, "Mucoadhesive polymers in the treatment of dry X syndrome," *Drug Discov Today,* vol. 21, no. 7, pp. 1051-62, Jul 2016, doi: 10.1016/j.drudis.2016.02.013.

[83] M. Ijaz and A. Bernkop-Schnurch, "Preactivated thiomers: their role in drug delivery," *Expert Opin Drug Deliv,* vol. 12, no. 8, pp. 1269-81, Aug 2015, doi: 10.1517/17425247.2015.1005598.

[84] P. Baranowski, B. Karolewicz, M. Gajda, and J. Pluta, "Ophthalmic drug dosage forms: characterisation and research methods," *ScientificWorldJournal,* vol. 2014, p. 861904, 2014, doi: 10.1155/2014/861904.

[85] J. Iqbal, G. Shahnaz, S. Dunnhaupt, C. Muller, F. Hintzen, and A. Bernkop-Schnurch, "Preactivated thiomers as mucoadhesive polymers for drug delivery," *Biomaterials,* vol. 33, no. 5, pp. 1528-35, Feb 2012, doi: 10.1016/j.biomaterials.2011.10.021.

[86] I. Altinbasak, M. Arslan, R. Sanyal, and A. Sanyal, "Pyridyl disulfide-based thiol–disulfide exchange reaction: shaping the design of redox-responsive polymeric materials," *Polymer Chemistry,* vol. 11, no. 48, pp. 7603-7624, 2020, doi: 10.1039/d0py01215g.

[87] C. Muller, B. N. Ma, R. Gust, and A. Bernkop-Schnurch, "Thiopyrazole preactivated chitosan: combining mucoadhesion and drug delivery," *Acta Biomater,* vol. 9, no. 5, pp. 6585-93, May 2013, doi: 10.1016/j.actbio.2013.01.008.

[88] F. Hintzen, S. Hauptstein, G. Perera, and A. Bernkop-Schnurch, "Synthesis and in vitro characterization of entirely S-protected thiolated pectin for drug delivery," *Eur J Pharm Biopharm,* vol. 85, no. 3 Pt B, pp. 1266-73, Nov 2013, doi: 10.1016/j.ejpb.2013.09.017.

[89] J. Nowak, F. Laffleur, and A. Bernkop-Schnurch, "Preactivated hyaluronic acid: A potential mucoadhesive polymer for vaginal delivery," *Int J Pharm,* vol. 478, no. 1, pp. 383-389, Jan 15 2015, doi: 10.1016/j.ijpharm.2014.11.048.

[90] I. Shahzadi *et al.*, "Less Reactive Thiol Ligands: Key towards Highly Mucoadhesive Drug Delivery Systems," *Polymers (Basel),* vol. 12, no. 6, May 30 2020, doi: 10.3390/polym12061259.

[91] A. Mandal, R. Bisht, I. D. Rupenthal, and A. K. Mitra, "Polymeric micelles for ocular drug delivery: From structural frameworks to recent preclinical studies," *J Control Release,* vol. 248, pp. 96-116, Feb 28 2017, doi: 10.1016/j.jconrel.2017.01.012.

[92] N. Boehnke, "Degradable Hydrogels and Nanogels for the Delivery of Cells and Therapeutics," Doctor of Philosophy, Chemistry, University of California, Los Angeles, 2017.

[93] B. Tyler, D. Gullotti, A. Mangraviti, T. Utsuki, and H. Brem, "Polylactic acid (PLA) controlled delivery carriers for biomedical applications," *Adv Drug Deliv Rev,* vol. 107, pp. 163-175, Dec 15 2016, doi: 10.1016/j.addr.2016.06.018.

[94] H. Peng *et al.*, "Reactive Copolymers Based on N-Vinyl Lactams with Pyridyl Disulfide Side Groups via RAFT Polymerization and Postmodification via Thiol–Disulfide Exchange Reaction,"

Macromolecules, vol. 49, no. 19, pp. 7141-7154, 2016, doi: 10.1021/acs.macromol.6b01210.

[95] J. Aguiar, P. Carpena, J. A. Molina-Bolívar, and C. Carnero Ruiz, "On the determination of the critical micelle concentration by the pyrene 1:3 ratio method," *Journal of Colloid and Interface Science,* vol. 258, no. 1, pp. 116-122, 2003, doi: 10.1016/s0021-9797(02)00082-6.

[96] S. Rossi, B. Vigani, M. C. Bonferoni, G. Sandri, C. Caramella, and F. Ferrari, "Rheological analysis and mucoadhesion: A 30 year-old and still active combination," (in eng), *J Pharm Biomed Anal,* vol. 156, pp. 232-238, Jul 15 2018, doi: 10.1016/j.jpba.2018.04.041.

[97] G. Moad, E. Rizzardo, and S. H. Thang, "Radical Addition–Fragmentation Chemistry and RAFT Polymerization," in *Polymer Science: A Comprehensive Reference*, 2012, pp. 181-226.

[98] C. Lote, *Principles Of Renal Physiology*. Springer, 2012, pp. 34-46.

[99] S. C. Owen, D. P. Y. Chan, and M. S. Shoichet, "Polymeric micelle stability," *Nano Today,* vol. 7, no. 1, pp. 53-65, 2012, doi: 10.1016/j.nantod.2012.01.002.

[100] L. Meli, J. M. Santiago, and T. P. Lodge, "Path-Dependent Morphology and Relaxation Kinetics of Highly Amphiphilic Diblock Copolymer Micelles in Ionic Liquids," *Macromolecules,* vol. 43, no. 4, pp. 2018-2027, 2010, doi: 10.1021/ma902366c.

[101] C. Di Tommaso, A. Torriglia, P. Furrer, F. Behar-Cohen, R. Gurny, and M. Moller, "Ocular biocompatibility of novel Cyclosporin A formulations based on methoxy poly(ethylene glycol)-hexylsubstituted poly(lactide) micelle carriers," *Int J Pharm,* vol. 416, no. 2, pp. 515-24, Sep 20 2011, doi: 10.1016/j.ijpharm.2011.01.004.

[102] T. Chakraborty, I. Chakraborty, and S. Ghosh, "The methods of determination of critical micellar concentrations of the amphiphilic systems in aqueous medium," *Arabian Journal of Chemistry,* vol. 4, no. 3, pp. 265-270, 2011, doi: 10.1016/j.arabjc.2010.06.045.

[103] L. Pineiro, M. Novo, and W. Al-Soufi, "Fluorescence emission of pyrene in surfactant solutions," *Adv Colloid Interface Sci,* vol. 215, pp. 1-12, Jan 2015, doi: 10.1016/j.cis.2014.10.010.

[104] N. Mangiacotte, G. Prosperi-Porta, L. Liu, M. Dodd, and H. Sheardown, "Mucoadhesive Nanoparticles for Drug Delivery to the Anterior Eye," *Nanomaterials (Basel),* vol. 10, no. 7, Jul 18 2020, doi: 10.3390/nano10071400.

[105] J. Griessinger *et al.*, "Methods to determine the interactions of micro- and nanoparticles with mucus," *Eur J Pharm Biopharm,* vol. 96, pp. 464-76, Oct 2015, doi: 10.1016/j.ejpb.2015.01.005.

[106] M. C. Bonferoni *et al.*, "Comparison of different in vitro and ex vivo methods to evaluate mucoadhesion of glycol-palmitoyl chitosan micelles," *Journal of Drug Delivery Science and Technology,* vol. 20, no. 6, pp. 419-424, 2010, doi: 10.1016/s1773-2247(10)50073-x.

[107] T. Eshel-Green and H. Bianco-Peled, "Mucoadhesive acrylated block copolymers micelles for the delivery of hydrophobic drugs," *Colloids Surf B Biointerfaces,* vol. 139, pp. 42-51, Mar 1 2016, doi: 10.1016/j.colsurfb.2015.11.044.

[108] V. M. de Oliveira Cardoso, M. P. D. Gremiao, and B. S. F. Cury, "Mucin-polysaccharide interactions: A rheological approach to evaluate the effect of pH on the mucoadhesive properties," *Int J Biol Macromol,* vol. 149, pp. 234-245, Apr 15 2020, doi: 10.1016/j.ijbiomac.2020.01.235.

[109] H. Hägerström and K. Edsman, "Limitations of the rheological mucoadhesion method: The effect of the choice of conditions and the rheological synergism parameter," *European Journal of Pharmaceutical Sciences,* vol. 18, no. 5, pp. 349-357, 2003, doi: 10.1016/s0928-0987(03)00037-x.

[110] J. A. Clayton, "Dry Eye," *N Engl J Med,* vol. 378, no. 23, pp. 2212-2223, Jun 7 2018, doi: 10.1056/NEJMra1407936.

[111] Z. Abedinzadeh, M. Gardes-Albert, and C. Ferradini, "Kinetic study of the oxidation mechanism of glutathione by hydrogen peroxide in neutral aqueous medium," *Can. J. Chem.,* vol. 67, pp. 1247-1255, 1988.

[112] J. R. Falck, B. Sangras, and J. H. Capdevila, "Preparation of N-tBoc L-glutathione dimethyl and di-tert-butyl esters: versatile synthetic building blocks," *Bioorg Med Chem,* vol. 15, no. 2, pp. 1062-6, Jan 15 2007, doi: 10.1016/j.bmc.2006.10.022.

[113] Y. Suga, H. Sunayama, T. Ooya, and T. Takeuchi, "Molecularly imprinted polymers prepared using protein-conjugated cleavable monomers followed by site-specific post-imprinting introduction of fluorescent reporter molecules," *Chem Commun (Camb),* vol. 49, no. 76, pp. 8450-2, Oct 4 2013, doi: 10.1039/c3cc40484f.

Appendix A - Monomer Synthesis

A1. GDSMA

A1.1. Methods

Synthesis of GDSMA was attempted using the 5-step synthesis shown in Figure A1 below.

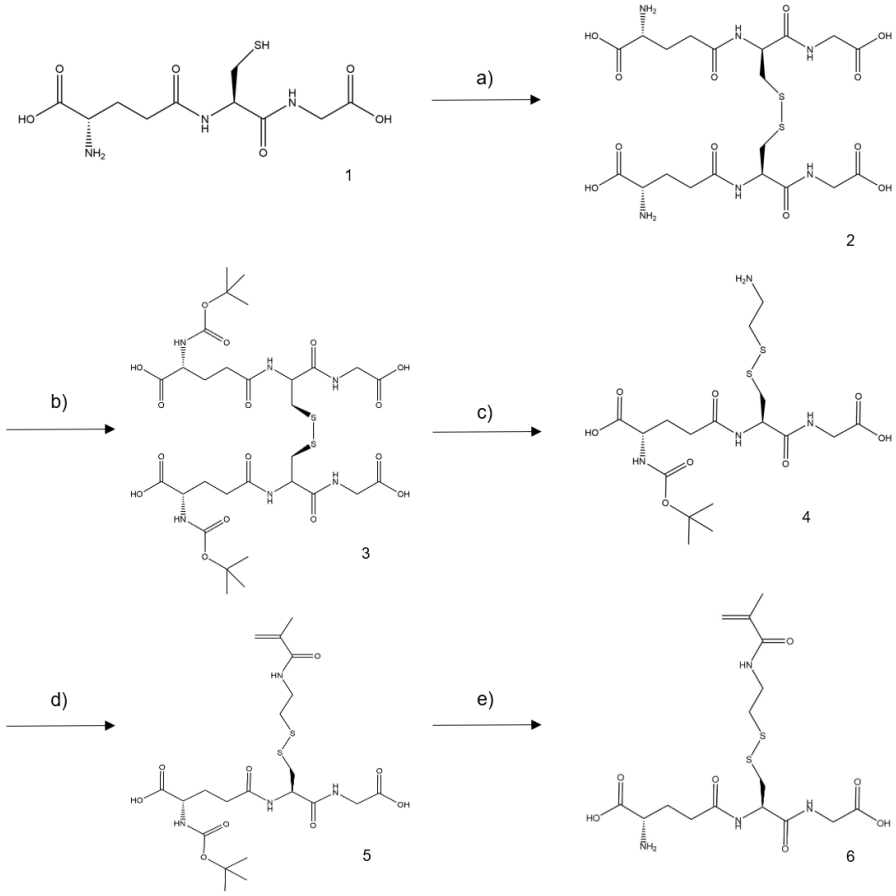

Figure A1. Synthesis of GDSMA monomer (**6**): a) H_2O_2, H_2O, 5 hr [111]; b) di-*tert*-butyl dicarbonate/$NaHCO_3$, Acetone/H_2O, 14 h [112]; c) Cysteamine, H_2O, N_2, pH 9.5, 24 hr; d) *N*-(methacryloxy)succinimide, PBS (0.1M, pH 7.4), 4°C, 24 hr; e) Trifluoroacetic acid (TFA), DCM, 24 hr.

Oxidized Glutathione (**2**)

L-Glutathione reduced (0.500 g, 1.63 mmol) was dissolved in water (15 mL). A 30% (w/w) H_2O_2 solution (0.174 mL, 1.71 mmol) was added to the stirring solution of L-Glutathione and pH was adjusted to 7.0 with 1M NaOH. The reaction mixture was left stirring for 5 hours, then lyophilized for 2 days to get **2**. Yield: 0.500 g (~ 100%). ^{1}H NMR (Bruker AV 600 MHz, D_2O): δ [ppm] = 4.78-4.76 ($SCH_2C\boldsymbol{H}$), 3.83-3.80 ($NHC\boldsymbol{H_2}C(=O)OH$), 3.79-3.76 ($NH_2C\boldsymbol{H}$), 3.34-3.31 and 3.01-2.97 ($SC\boldsymbol{H_2}CH$), 2.60-2.51 ($NHC(=O)C\boldsymbol{H_2}CH_2$), 2.20-2.16 ($NHC(=O)CH_2C\boldsymbol{H_2}$).

[*N*,*N'*-bis(*tert*-butoxycarbonyl)](oxidized glutathione) [$(BocGS)_2$] (**3**)

Compound **2** (0.500 mg, 0.82 mmol) and $NaHCO_3$ (0.274 g, 3.26 mmol) were dissolved in 2.4:1 tetrahydrofuran (THF)/H_2O (7.5 mL). A solution of Di-*tert*-butyl dicarbonate (0.427 g, 1.96 mmol) in 2.4:1 THF/H_2O (5 mL) was made and transferred to the stirring reaction mixture. The reaction was left stirring for 24 hours, followed by solvent volume reduction *in vacuo* to remove THF. The resulting aqueous phase was adjusted to pH 3.0 with 0.1M HCl and extracted with EtOAc (4 x 10 mL). Extractions were collected and dried with $MgSO_4$, gravity filtered, and product was concentrated *in vacuo* to give Compound **3** as a colourless oil. Yield: 0.232 g (35.1%). ^{1}H NMR (Bruker AV 600 MHz, D_2O): δ [ppm] = 4.78-4.76 ($SCH_2C\boldsymbol{H}$), 4.10-4.09 ($NHC\boldsymbol{H}(C(=O)OH)$), 4.01 ($NHC\boldsymbol{H_2}C(=O)OH$), 3.29-3.27 and 2.99-2.95 ($SC\boldsymbol{H_2}CH$), 2.48 ($NHC(=O)C\boldsymbol{H_2}CH_2$), 2.19 and 1.97 ($NHC(=O)CH_2C\boldsymbol{H_2}$), 1.44 ($C(CH_3)_3$).

N-tert-butoxycarbonylglutathione(cysteamine) [Boc-GSH-Cys] (**4**)

Cysteamine (0.029 g, 0.38 mmol) was dissolved in purified water (12.5 mL) in an oven dried flask. Compound **3** (0.232 g, 0.29 mmol) was dissolved in purified water (12.5 mL) and added to the reaction mixture. pH was adjusted to 9.5 with 1M NaOH followed by purging with N_2. Reaction was stirred for 24 hours, then pH was lowered to 3.0 with 1M HCl, followed by extractions with EtOAc (5 x 10 mL). Aqueous phase volume was reduced *in vacuo* to obtain an impure Compound **4** as a colourless oil. Yield: 0.011 g (~ 8%). ^{1}H NMR (Bruker AV 600 MHz, D_2O): δ [ppm] = 4.78-4.76 ($SCH_2C\boldsymbol{H}$), 4.06 (NHC***H***(C(=O)OH)), 3.95 (NHC***H₂***C(=O)OH), 3.39 ($NH_2C\boldsymbol{H_2}CH_2$), 3.31-3.28 and 3.04-2.95 ($SC\boldsymbol{H_2}CH$), 3.11-3.05 and 2.69-2.66 ($NH_2CH_2C\boldsymbol{H_2}$), 2.47 ($NHC(=O)C\boldsymbol{H_2}CH_2$), 2.17 and 1.95 ($NHC(=O)CH_2C\boldsymbol{H_2}$), 1.44 ($C(CH_3)_3$).

N-tert-butoxycarbonyl(glutathione disulfide ethyl methacrylate) [Boc-GDSMA] (**5**)

Compound **4** (~ 0.011 g, 22.80 µmol) along with the impurities from reaction (c) were dissolved in 7.5 mL of PBS (0.1M, pH 7.4). *N*-(Methacryloyloxy)succinimide (NMAS; 0.007 g, 34.20 µmol) stock solution was prepared in PBS (0.1M, pH 7.4) to a concentration of 10 mg/mL and the required mass of NMAS was transferred to the stirring reaction by volume. pH was adjusted to 7.4 with 1M NaOH, and the reaction was left stirring for 24 hours, followed by volume reduction *in vacuo*. Resulting Compound **5** was purified by reducing the reaction mixture pH to 3.5

using 1M HCl, followed by extractions against EtOAc (3 x 10 mL). Resulting impure product aqueous phase volume was reduced *in vacuo* to obtain a yellow glue (Yield: undetermined).

A1.2. NMR & Electrospray Ionization Mass Spectrometry (ESI-MS) Results

The successful synthesis of purified Compounds **2** and **3** can be seen in Figure A2 and Figure **A3** below. The purification of both products was successful; however, the yield of Compound **3** was lower than expected and could make use of future optimization.

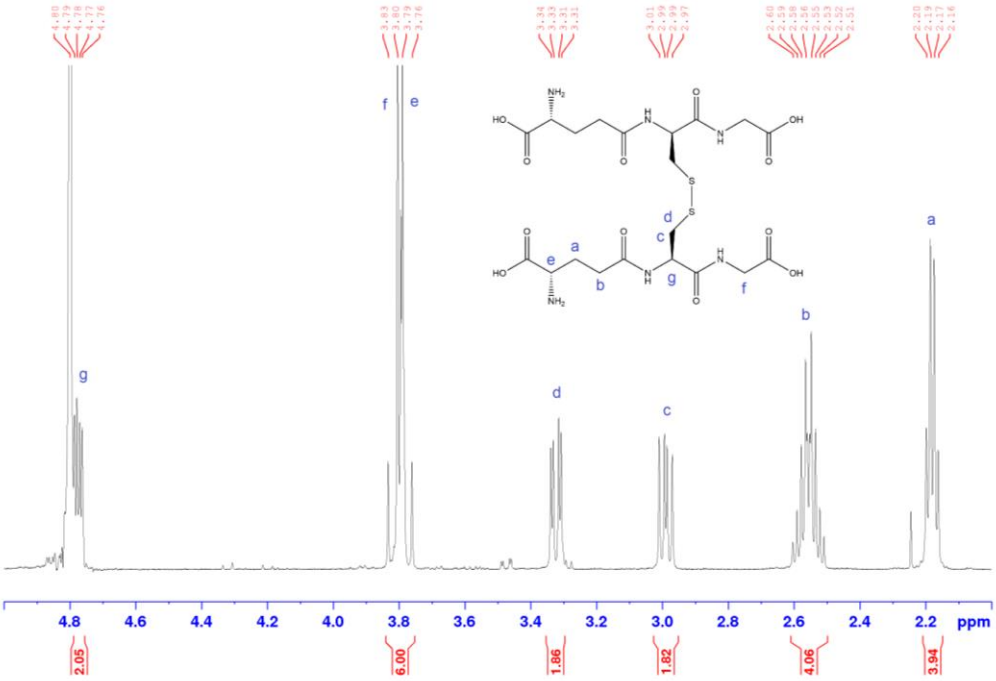

Figure A2. ^{1}H NMR spectrum of Compound 2 in D_2O.

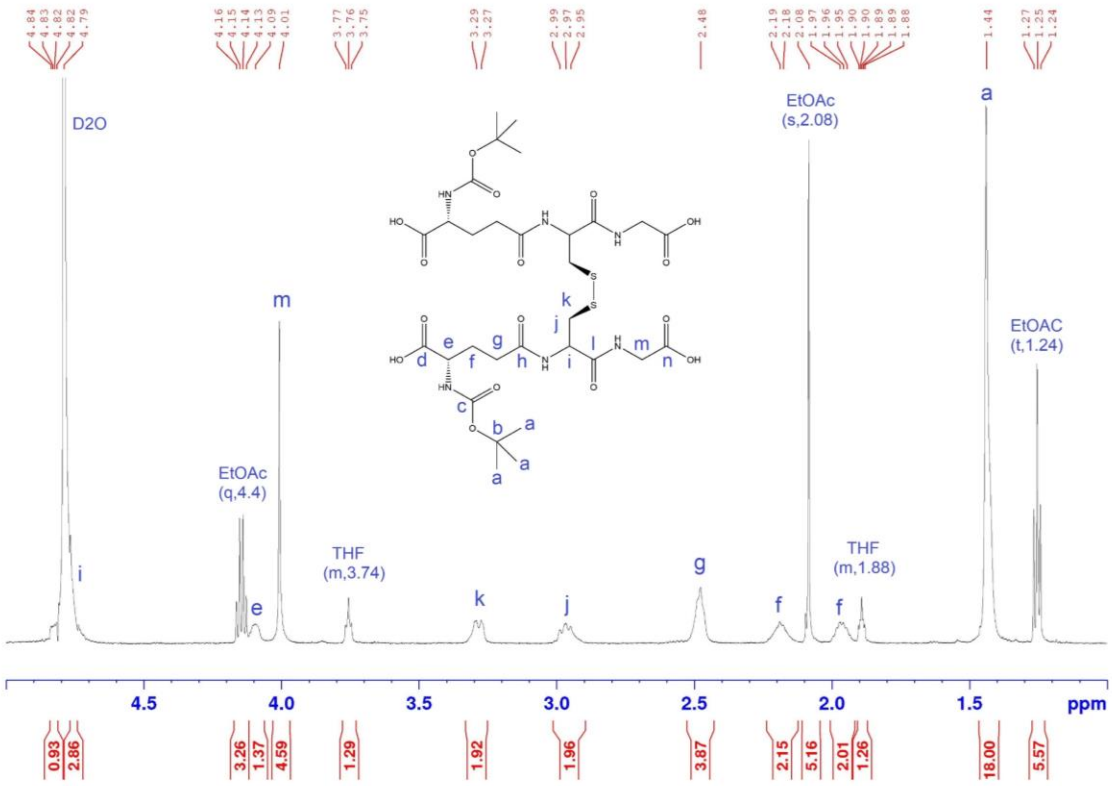

Figure A3. ^{1}H NMR spectrum of Compound 3 in D_2O.

The synthesis of Compound **4** was attempted, however difficulties with purification resulted in a low yield of ~ 8% and an impure final product as seen by the ^{1}H NMR spectrum in Figure A4. Silica column chromatography was attempted with column solvent 70:30 EtOAc/Acetic Acid but was unsuccessful as no separation was observed in the product eluted from the column. Therefore, future work would benefit from optimization of column solvents and potentially the use of a different column material to improve separation. In addition, reaction conditions could be investigated to determine whether the overall yield of product could be improved upon. It was determined however that the reaction was successful in

producing some amount of Compound **4** as seen in Figure A5 which shows the electrospray ionization mass spectrometry (ESI-MS) results from a sample made from the aqueous phase of the extractions showing the presence of Compound **4** in comparison to the theoretical model of Compound **4** generated by the software.

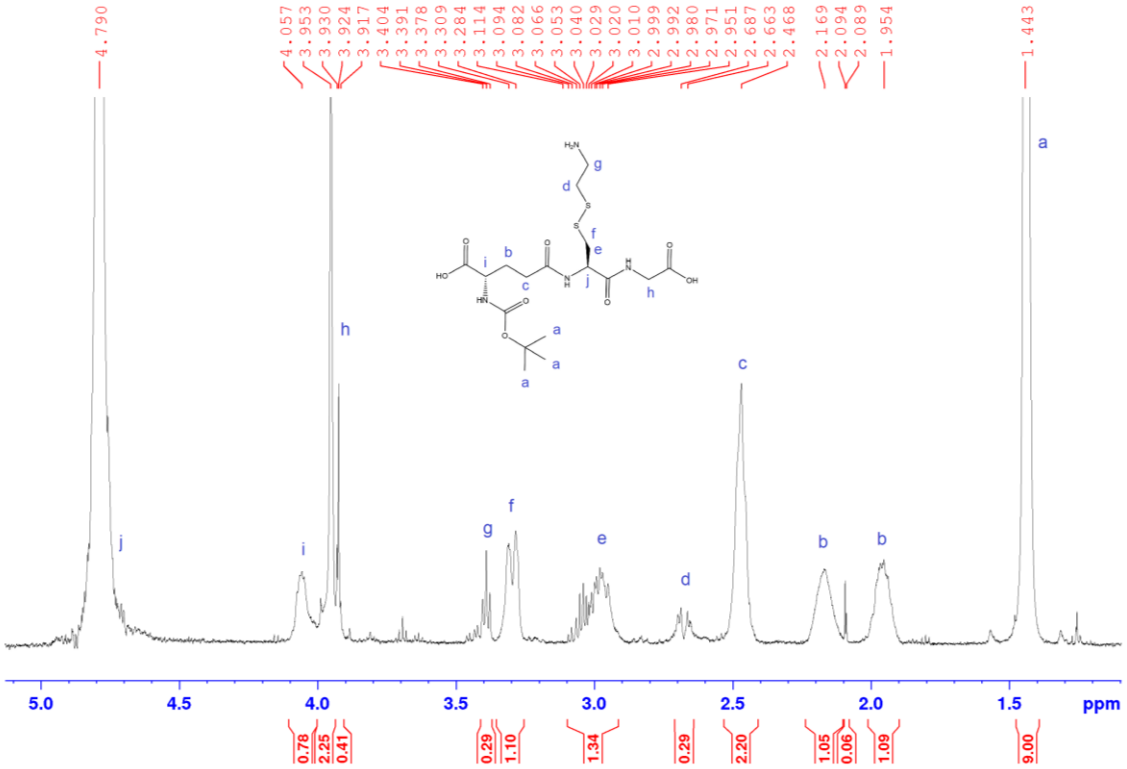

Figure A4. ^{1}H NMR spectrum of impure Compound 4 in D_2O.

An attempt at synthesizing Compound **5** was made, however there were issues again with purification. Extractions were unable to remove most by-products from reaction and resulted in an ^{1}H NMR that was difficult to analyze. For this reason, a sample of the organic phase of the extractions was made and analyzed with ESI-MS. Figure A6 shows the spectrum from this sample and its comparison to the

theoretical model for the ESI-MS spectrum of Compound **5**. As can be seen, the sample matches the theoretical model and so confirms the presence of Compound **5** in the sample and therefore that Compound **5** was indeed synthesized. However, due to problems with purification, no yield could be determined.

Due to the issues encountered with Compounds **4** and **5**, further work on the synthesis of Compound **6** was halted in favour of a different monomer discussed in the subsequent section.

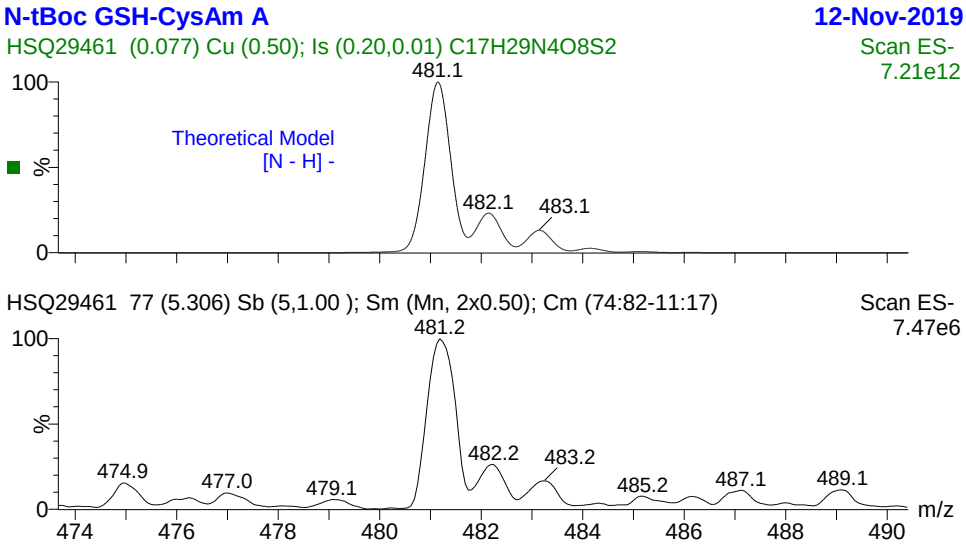

Figure A5. ESI-MS results of aqueous phase of extractions for Compound 4 showing the presence of Compound 4 in solution (bottom spectrum) in comparison to the theoretical model (top spectrum).

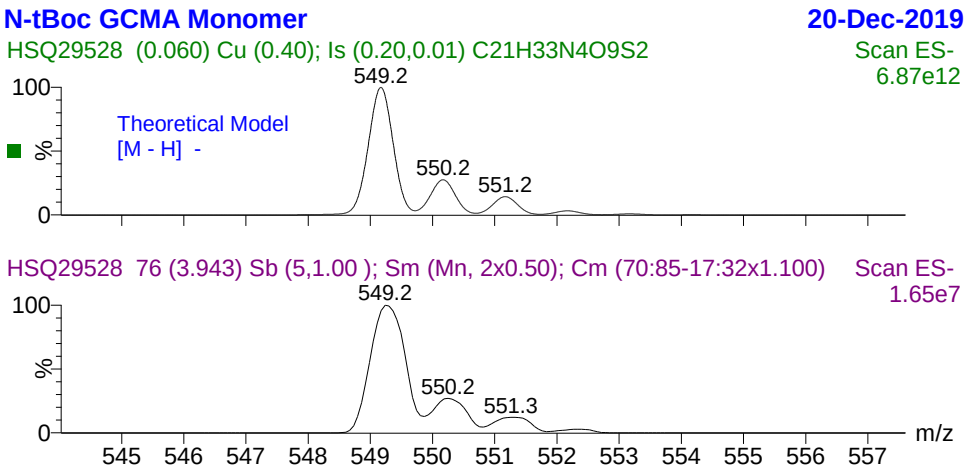

Figure A6. ESI-MS results of organic phase of extractions for Compound 5 showing the presence of Compound 5 in solution (bottom spectrum) in comparison to the theoretical model (top spectrum).

A2. MAC Method 1

The first attempt at the synthesis of MAC followed the 3-step synthesis shown in Figure A7 below [113].

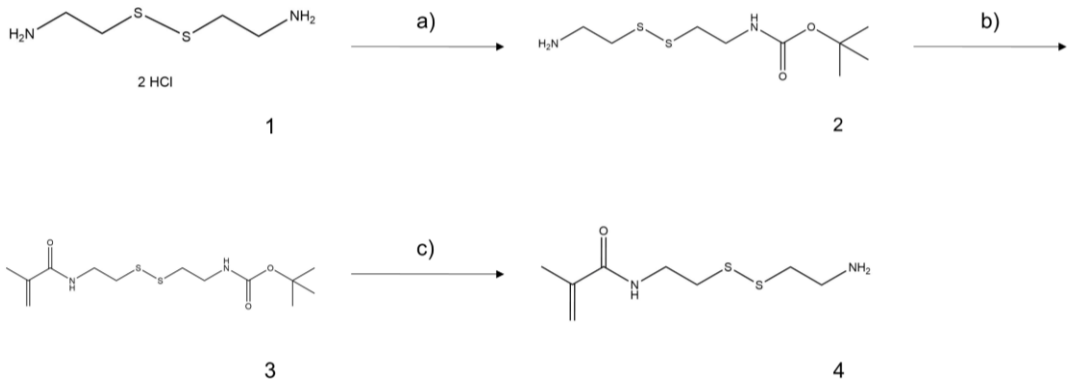

Figure A7. Synthesis of MAC monomer (**4**) scheme 1: a) di-*tert*-butyl dicarbonate/triethylamine, MeOH, 0°C, 6 hr, 73%; b) methacryloyl chloride/DIPEA, anhydrous DCM, 0°C, 24 hr, 66.8%; c) TFA, DCM, 17 hr, undetermined yield.

A2.1. Methods

Mono-boc Cystamine [MBC] (**2**)

Cystamine dihydrochloride (2.252 g, 10.00 mmol) and triethylamine (3.036 g, 30.00 mmol) were dissolved in MeOH (30 mL). A solution of di-*tert*-butyl dicarbonate (1.091 g, 5.00 mmol) in MeOH (20 mL) was made and added to the above reaction mixture. The reaction was allowed to stir for 6 hours, then solvent volume was reduced *in vacuo*. Crude product was redissolved in 1M NaH_2PO_4 and extractions were run against diethyl ether (2 x 20 mL). The aqueous extract was then pH adjusted to 9.0 by addition of 1M NaOH prior to extractions against ethyl acetate (3 x 20 mL). The organic phase extracts were collected and run against a brine wash (1 x 20 mL) followed by drying with $MgSO_4$, gravity filtering, and solvent volume reduction *in vacuo* to give the final product **2** as a yellow oil. Yield: 0.921 g (73%). ^{1}H NMR (Bruker AV 600 MHz, $CDCl_3$): δ [ppm] = 4.93 (N***H***-Boc), 3.45 (C***H₂***NH-Boc), 3.01 (NH_2C***H₂***CH_2), 2.79-2.75 (C***H₂***SSC***H₂***), 1.44 (C(C***H₃***)***₃***).

N-tert-butoxycarbonyl-*N'*-methacryloylcystamine [BMAC] (**3**)

Compound **2** (0.921 g, 3.65 mmol) and DIPEA (0.944 mg, 0.127 mL, 7.30 mmol) were dissolved in anhydrous DCM (30 mL) and cooled to 0°C. Methacryloyl chloride (0.496 g, 0.496 µL, 4.75 mmol) was dissolved in anhydrous DCM (30 mL) and added dropwise to the above solution and allowed to react for 24 hours. The reaction mixture was washed with brine (2 x 30 mL), dried with $MgSO_4$, gravity

filtered, then solvent volume reduced *in vacuo*. The crude product was purified with silica gel column chromatography (1:1 Hexanes/EtOAc). Compound **3** was obtained as a yellow powder. Yield: 0.782 g (66.8%). TLC: R_f 0.30 (1:1 Hexanes/EtOAc). ^{1}H NMR (Bruker AV 600 MHz, $CDCl_3$): δ [ppm] = 6.44 (N***H***C(=O)C(=CH_2)CH_3), 5.74 and 5.35 (C(=C***H₂***)), 4.96 (N***H***-Boc), 3.65 (C***H₂***NHC(=O)C(=CH_2)CH_3), 3.45 (C***H₂***NH-Boc), 2.88 (C***H₂***CH_2NHC(=O)C(=CH_2)CH_3), 2.80 (C***H₂***CH_2NH-Boc), 1.97 (C(=CH_2)C***H₃***), 1.44 (C(C***H₃***)***₃***).

N-methacryloylcystamine [MAC] (**4**)

Compound **3** (0.150 g, 0.47 mmol) was dissolved in DCM (1.5 mL) and TFA (1.5 mL) was added to the solution. Reaction was left to stir overnight, then solvent volume was reduced *in vacuo* to obtain Compound **4** as a crude product. Yield: undetermined. ^{1}H NMR (Bruker AV 600 MHz, $CDCl_3$): δ [ppm] = 8.01 (N***H₂***CH_2), 6.34 (C(=O)N***H***), 5.77 and 5.44 (CH_3C(=C***H₂***)), 3.68 (NHC***H₂***), 3.42 (NH_2C***H₂***), 3.14 (NHCH_2C***H₂***), 2.89 (NH_2CH_2C***H₂***), 1.95 (C***H₃***C(=CH_2)).

A2.2. NMR Results

The successful synthesis of Compounds **2**, **3**, and **4** are reported in the ^{1}H NMR spectrums in Figure A8, Figure **A9**, and Figure **A10** below. Yields of both Compounds **2** and **3** were found to agree with or even exceed literature sources. However, issues with the purification of Compound **4** were experienced. A superior

method, requiring only 2 reaction steps, as opposed to the 3 reaction steps required here, was proposed, and attempted next.

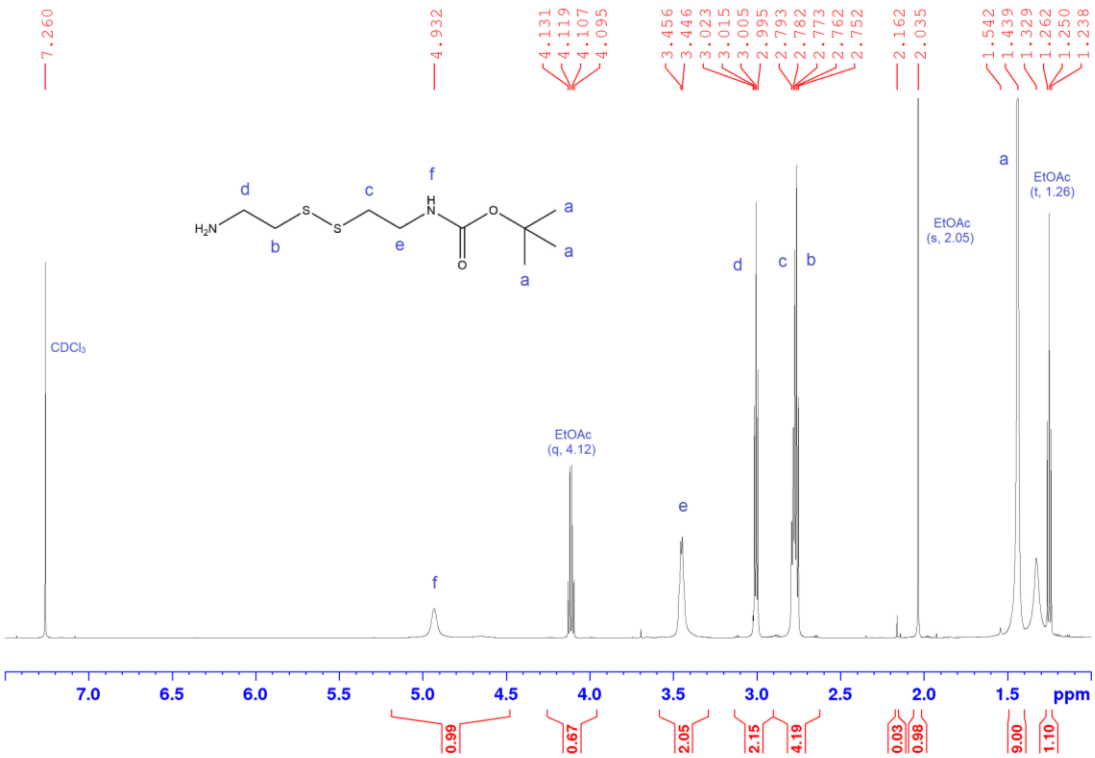

Figure A8. ^{1}H NMR spectrum for Compound 2 in $CDCl_3$.

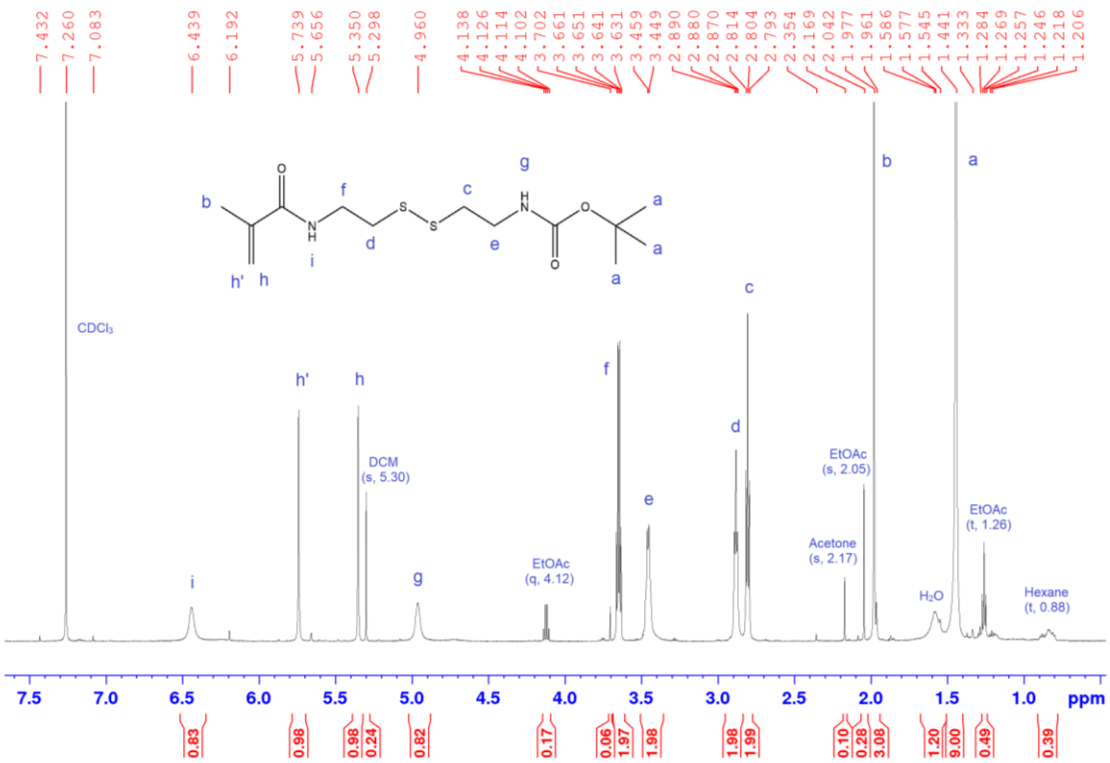

Figure A9. ^{1}H NMR spectrum of Compound 3 in $CDCl_3$.

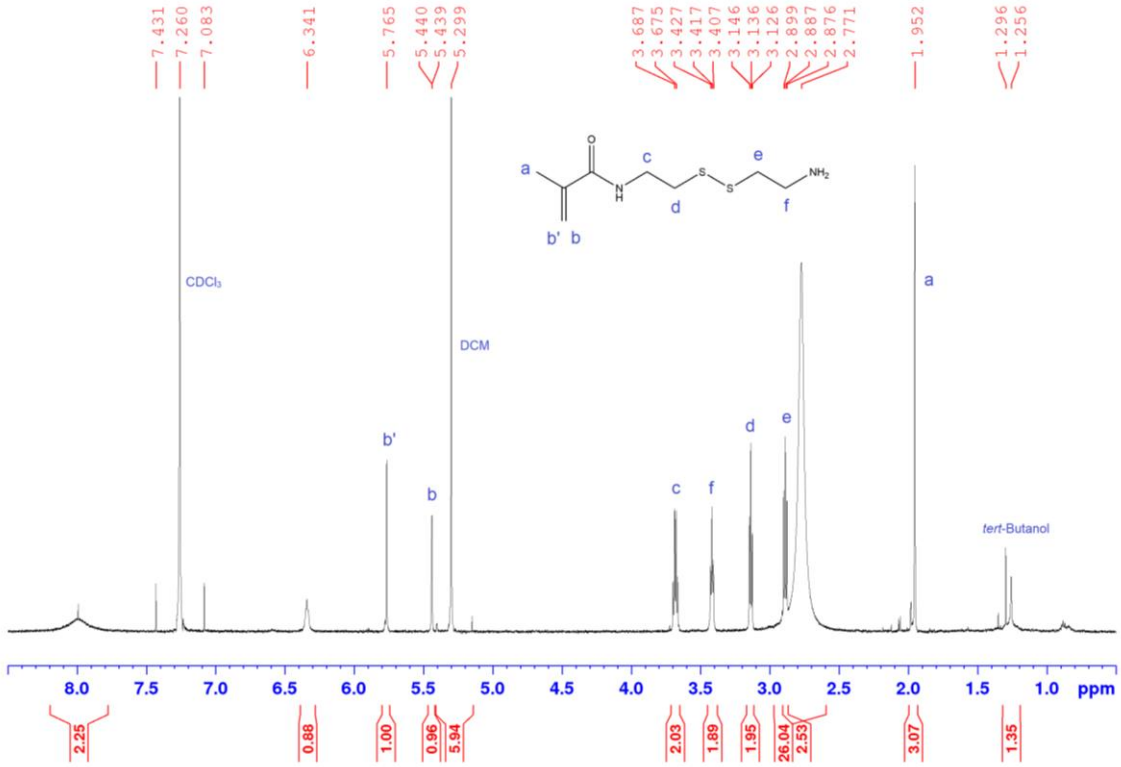

Figure A10. ^{1}H NMR spectrum of Compound 4 in $CDCl_3$.

A3. MAC Method 2

The second attempt at the synthesis of MAC used the 2-step synthesis shown in Figure A11 below.

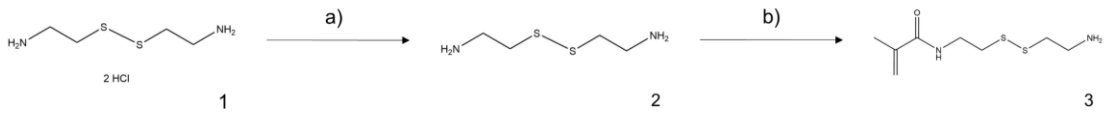

Figure A11. Synthesis of MAC monomer (**3**) scheme 2: a) NaOH, Water, 2.5 hrs; b) Methacryloyl Chloride/DIPEA, anhydrous DCM, 0°C, 24 hrs.

A3.1. Methods

Cystamine (**2**)

Cystamine dihydrochloride (0.766 mg, 3.40 mmol) was dissolve in 50 mL of water. NaOH (0.408 mg, 10.20 mmol) was added to the stirring solution and allowed to react for 1.5 hours. Solvent volume was reduced *in vacuo*, then 50 mL of DCM was added to the crude product to precipitate the salt and dissolve the product. The organic layer was dried with $MgSO_4$ and gravity filtered. Solvent volume was removed *in vacuo* to obtain Compound **2** as a brown oil. Yield: 0.352 mg (68%).

N-Methacryloyl Cystamine [MAC] (**3**)

Compound **2** (0.564 g, 3.71 mmol) containing water (0.085 g, 4.73 mmol), was mixed with DIPEA (2.180 g, 2.94 mL, 16.87 mmol) in anhydrous DCM (20 mL) and cooled to 0°C. Methacryloyl chloride (1.146 g, 1.07 mL, 10.96 mmol) was dissolved in anhydrous DCM (30 mL) and added dropwise to the above solution and allowed to react for 24 hours. The reaction mixture was washed with brine (3 x 25 mL), dried with $MgSO_4$, gravity filtered, then solvent volume reduced *in vacuo*. Compound **3** was not obtained, and instead a crude bis(methacryloyl)cystamine product was obtained as a yellow powder. Yield: undetermined. ^{1}H NMR (Bruker AV 600 MHz, $CDCl_3$): δ [ppm] = 6.47 (N***H***C(=O)C(=CH_2)CH_3), 5.74 and 5.35 (C(=C***H₂***)), 3.65 (C***H₂***CH_2SSCH_2C***H₂***), 2.88 (CH_2C***H₂***SSC***H₂***CH_2), 1.97 (C(=CH_2)C***H₃***).

A3.2. NMR Results

The successful synthesis of Compound **2** was determined by NMR and by the success of the purification method, whereby any cystamine devoid of its salt would dissolve in DCM, while any remaining unreacted cystamine dihydrochloride would precipitate as a salt along with any NaCl byproduct resulting from the reaction.

Synthesis of Compound **3** was unsuccessful and instead the di-acrylate was synthesized namely bis(methacryloyl)cystamine (spectrum shown in Figure A12). During the purification of cystamine from its salt in the previous step, there was difficulty removing all the water from the cystamine and therefore to account for this additional reactant in the subsequent step, additional methacryloyl chloride was added to the reaction, since it to can react with methacryloyl chloride. The initial desire was to mono-functionalize cystamine with methacryloyl chloride using 1.3 molar equivalents. However, this additional methacryloyl chloride resulted in ~ 3 molar equivalents in comparison to cystamine (1.3 molar equivalents were used overall in comparison to the amount of both cystamine and water in the sample). If the methacryloyl chloride preferentially reacted with the cystamine, then this would have been more than enough to di-functionalize it in theory. Therefore, future work should investigate the purification method for the first step to remove more water, potentially lyophilizing the cystamine product. Additionally, future work should investigate optimizing the purification of the resulting methacryloyl cystamine using extractions and column chromatography.

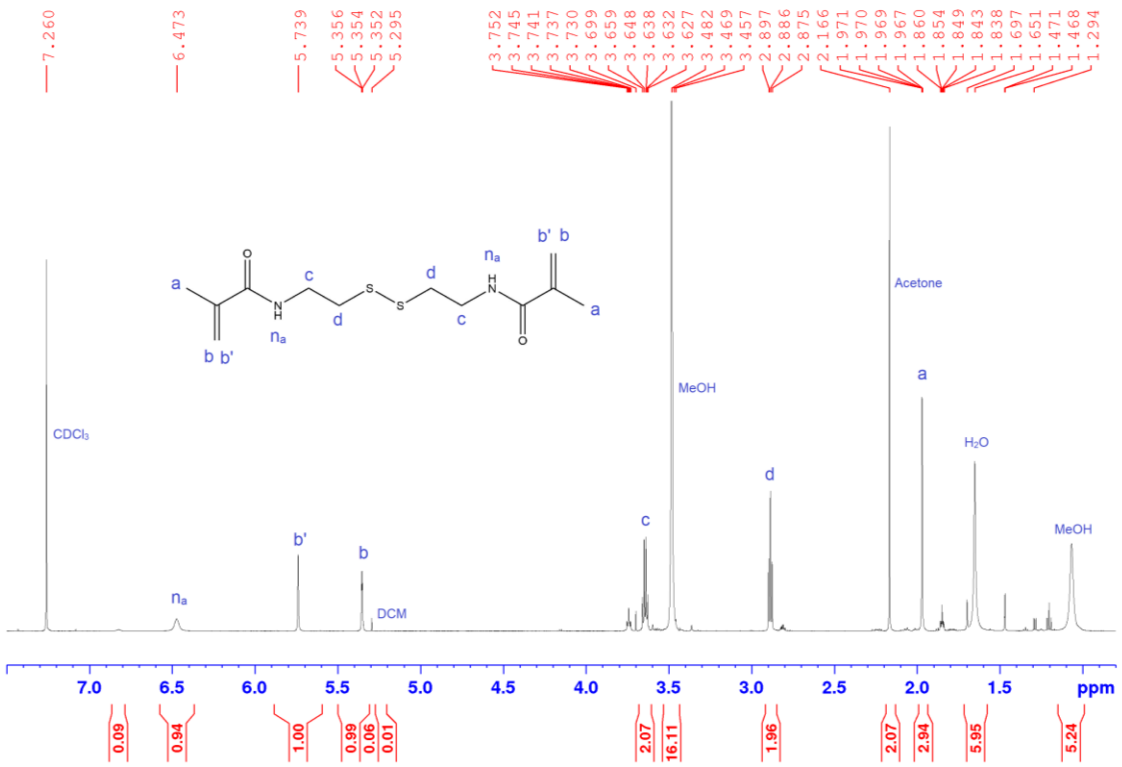

Figure A12. ^{1}H NMR spectrum for bis(methacryloyl)cystamine in $CDCl_3$.

Due to the problems experienced with both MAC methods, the synthesis of PDSMA was chosen moving forward as it was worked on in tandem and was more successful. In addition, the PDSMA monomer allowed for more versatility in future work with the ability to post-modify polymers containing the PSDMA monomer with a wealth of small thiol molecules through a thiol/disulfide exchange reaction. Therefore, work on the optimization and successful synthesis of the MAC monomer was halted.

Appendix B - Post-Polymerization Modification

Successful attempts at the post-polymerization modification of the LMS-20 polymer with small thiol molecules GSH (LMG-20) and Cys (LMC-20) are reported in Figure B1 and Figure **B2**.

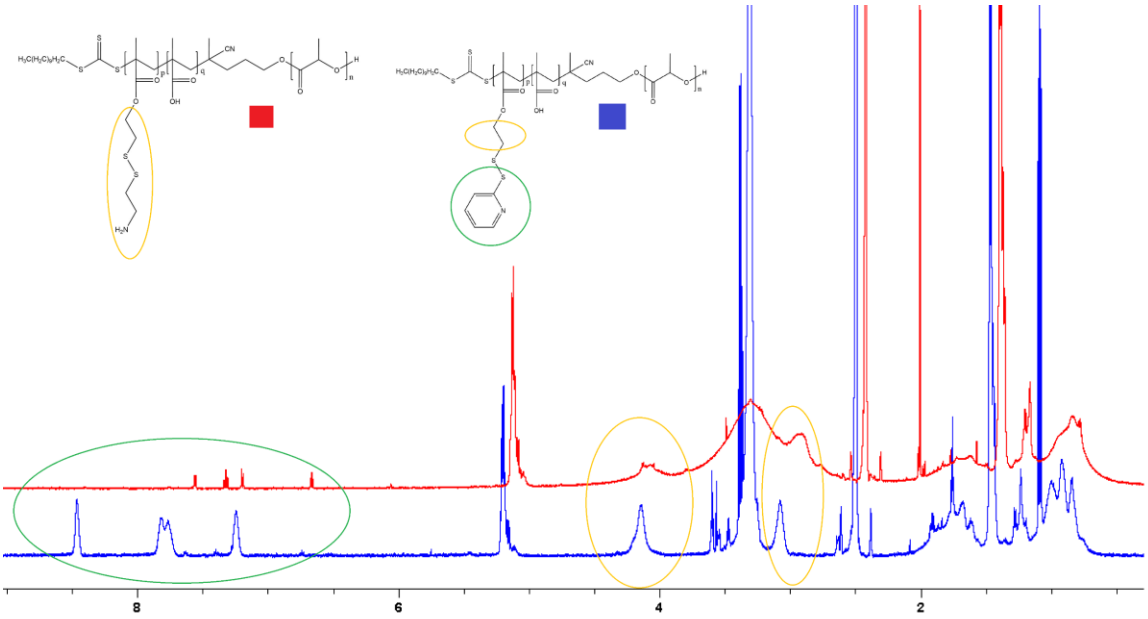

Figure B1. ^{1}H NMR spectra comparison between LMS-20 (blue) and LMC-20 (red). Yellow circles represent the peaks attributable to the successful modification with Cys; green circles represent the peaks of the PDS group that can be seen to have significantly diminished (only 1 of 25 PDS groups remain) following successful modification.

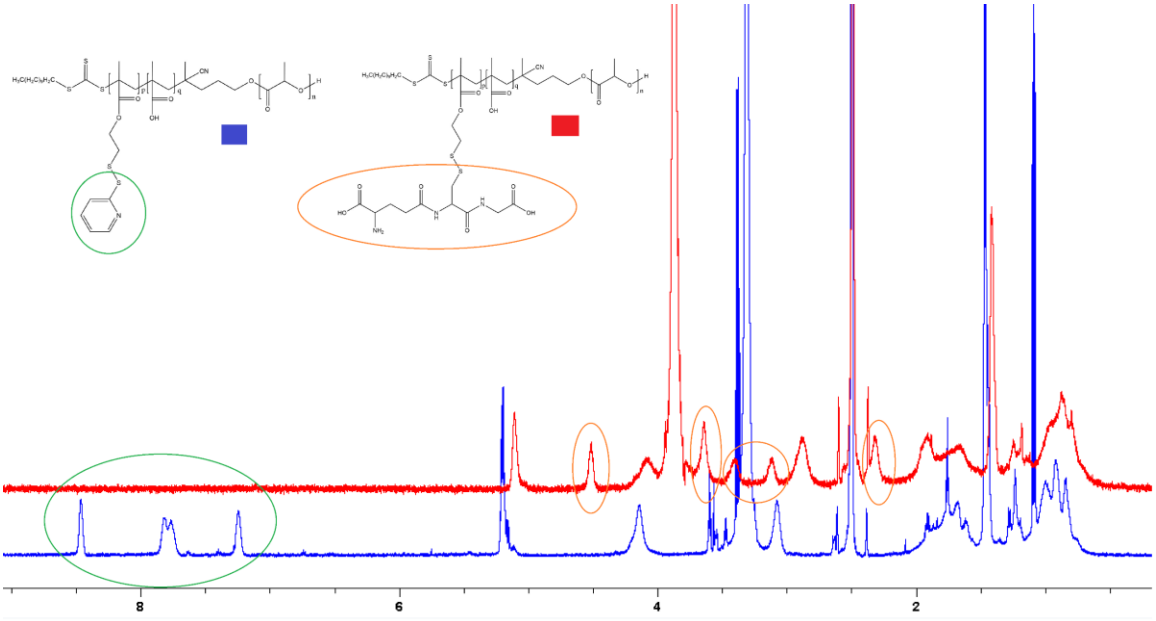

Figure B2. ^{1}H NMR spectra comparison between LMS-20 (blue) and LMC-20 (red). Yellow circles represent the peaks attributable to the successful modification with GSH; green circles represent the peaks of the PDS group that can be seen to have been eliminated following successful modification.

The polymers LMC-20 and LMG-20 were not chosen for further testing for this thesis as there were difficulties in determining a suitable solvent for nanoprecipitations. It is believed that the primary amines are responsible for the difficulties in solubility in these two polymers, as the polymer LMA-20 which contains no primary amines was easily soluble in acetone/water for nanoprecipitations, whereas both LMC-20 and LMG-20 have a primary amine, along with LMG-20 having 2 carboxylic acids. Future work should look at an appropriate solvent system for nanoprecipitations and the prospect of using other small thiol molecules depending on the intended purpose of the delivery system.

Appendix C - Rheology

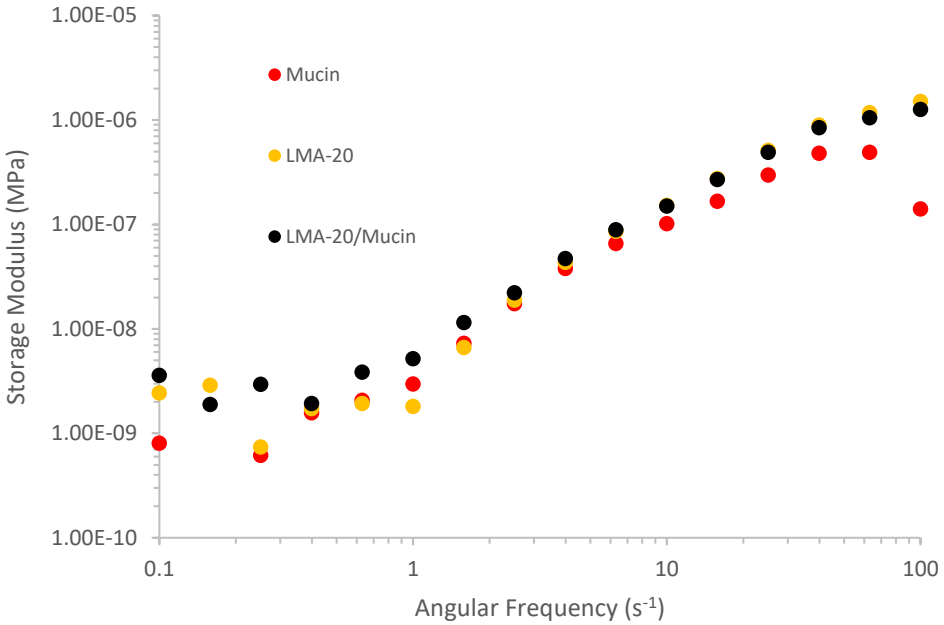

Figure C1. Oscillatory frequency sweep showing storage modulus of mucin, LMA-20, and LMA-20/mucin mixture at a strain of 1%. Each value represents the average of n=3 measurements. Error bars omitted for clarity.

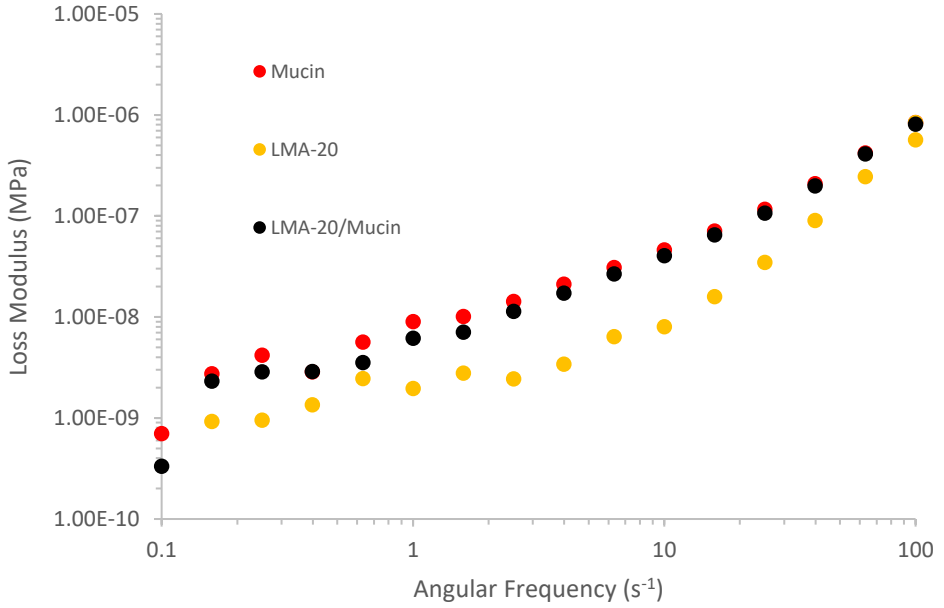

Figure C2. Oscillatory frequency sweep showing loss modulus of mucin, LMA-20, and LMA-20/mucin mixture at a strain of 1%. Each value represents the average of n=3 measurements. Error bars omitted for clarity.

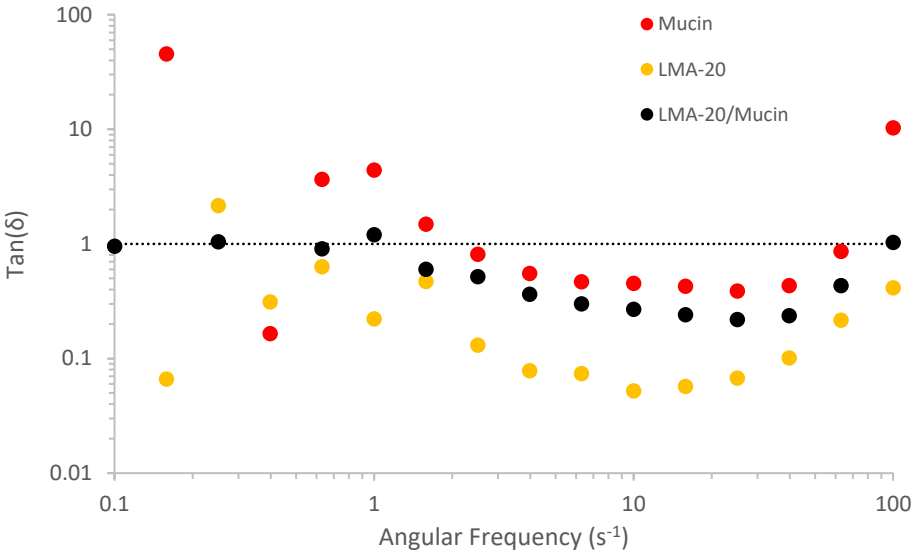

Figure C3. Oscillatory frequency sweep showing damping factor of mucin, LMA-20, and LMA-20/mucin mixture at a strain of 1%. Each value represents the average of n=3 measurements. Error bars omitted for clarity.

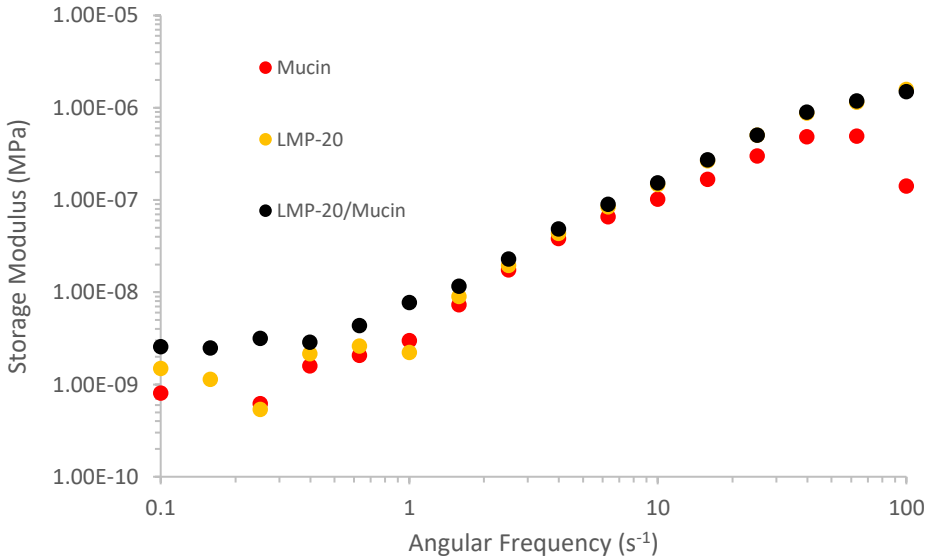

Figure C4. Oscillatory frequency sweep showing storage modulus of mucin, LMP-20, and LMP-20/mucin mixture at a strain of 1%. Each value represents the average of n=3 measurements. Error bars omitted for clarity.

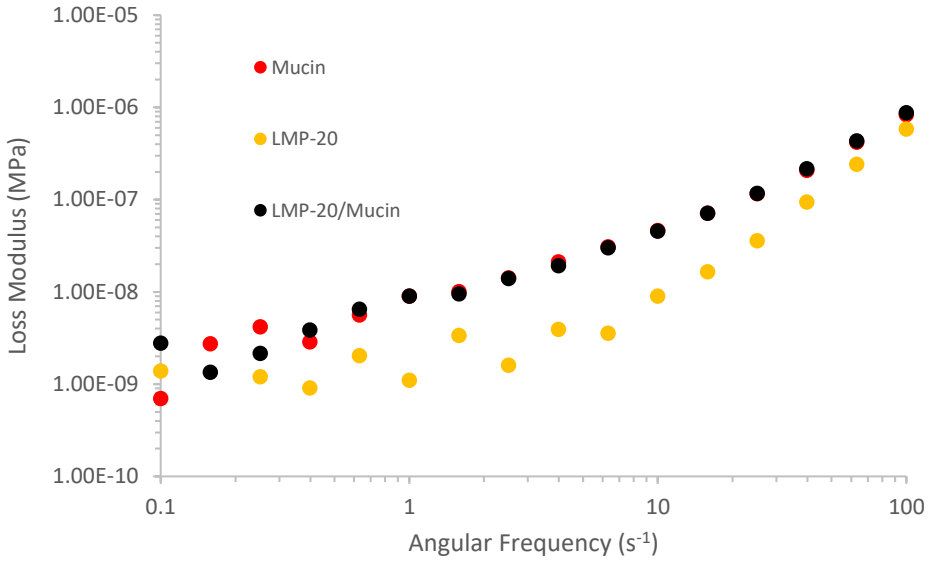

Figure C5. Oscillatory frequency sweep showing loss modulus of mucin, LMP-20, and LMP-20/mucin mixture at a strain of 1%. Each value represents the average of n=3 measurements. Error bars omitted for clarity.

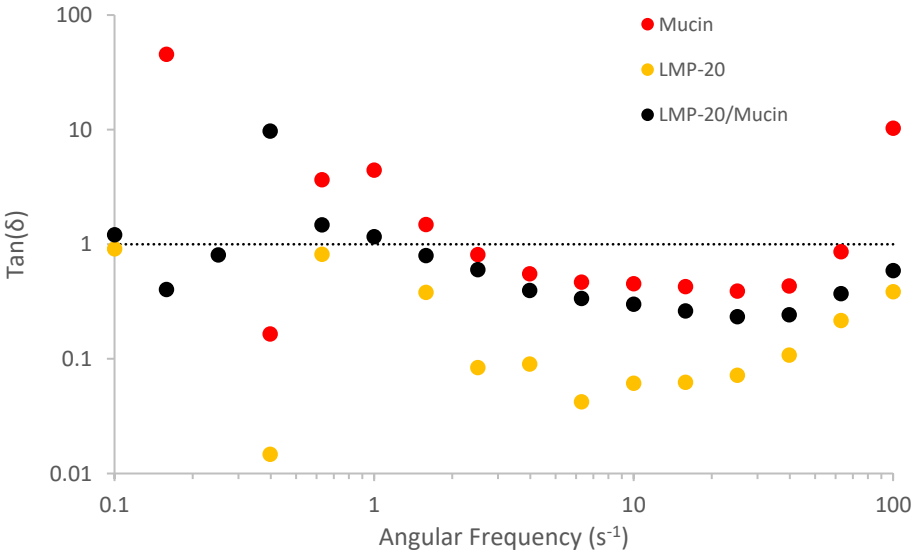

Figure C6. Oscillatory frequency sweep showing damping factor of mucin, LMP-20, and LMP-20/mucin mixture at a strain of 1%. Each value represents the average of n=3 measurements. Error bars omitted for clarity.